



SCHOOL OF COMPUTER SCIENCE

BioPixel: Investigating Bio-compatibile Materials for Wearable Eink Display Fabrication

Alexander Bloom

A dissertation submitted to the University of Bristol in accordance with the requirements of the degree
of Bachelor of Science in the Faculty of Engineering **worth 40CP**.

Thursday 1st May, 2025

Abstract

BioPixel explores the development of a wearable E-Ink display using biocompatible E-Ink microcapsules embedded in a conductive hydrogel substrate. This project builds on home-made E-Ink microcapsules developed in Bristol. While these capsules are functional, they are still in the early stages of development, and it remains unclear how to embed them into materials suitable for wearable displays. As such, the project is rooted in chemistry, biology, and materials science to explore the potential integration of these microcapsules into functional wearable systems.

We appraise technical literature to consolidate foundational knowledge across biocompatibility testing, hydrogel design and electrophoretic display integration. We develop a conductive hydrogel that can be used in wearable electronic displays. We identify a key roadblock to the creation of a wearable E-Ink display, the fragility and poor UV stability of the current generation of biocompatible E-Ink microcapsules, and propose future development strategies to overcome these limitations. By addressing the gap between recent advances in biocompatible electrophoretic materials, flexible conductive materials, and the vision of a wearable E-Ink display we lay the foundation for the future realisation of a wearable E-Ink display and, ultimately, "digital tattoos".

Declaration

I declare that the work in this dissertation was carried out in accordance with the requirements of the University's Regulations and Code of Practice for Taught Programmes and that it has not been submitted for any other academic award. Except where indicated by specific reference in the text, this work is my own work. Work done in collaboration with, or with the assistance of others including AI methods, is indicated as such. I have identified all material in this dissertation which is not my own work through appropriate referencing and acknowledgement. Where I have quoted or otherwise incorporated material which is the work of others, I have included the source in the references. Any views expressed in the dissertation, other than referenced material, are those of the author.

Alexander Bloom, Thursday 1st May, 2025

AI Declaration

I declare that any and all AI usage within the project has been recorded and noted within Appendix A or within the main body of the text itself. This includes (but is not limited to) usage of text generation methods incl. LLMs, text summarisation methods, or image generation methods.

I understand that failing to divulge use of AI within my work counts as contract cheating and can result in a zero mark for the dissertation or even requiring me to withdraw from the University.

Alexander Bloom, Thursday 1st May, 2025

Contents

1	Introduction	1
1.1	Motivation	1
1.2	Contributions	2
1.3	Teamwork Aspects	3
1.4	Report Organisation	3
2	Related Work on programmable ink fabrication	4
2.1	Programme Inks in HCI	4
2.2	E-Ink Microcapsules	5
2.3	Use of Hydrogel	6
2.4	Summary	6
3	Part 1: Biocompatibility	7
3.1	Introduction to Biocompatibility	7
3.2	Understanding the ISO 10993 Series	7
3.3	Implementing the ISO 10993 Series	8
3.4	Biocompatibility Testing of the Novel E-Ink Microcapsule	9
3.5	Results and Discussion	11
4	Part 2: Hydrogels	13
4.1	Introduction to Hydrogels	13
4.2	Classifying Hydrogels	13
4.3	Characterisation of Hydrogels	15
4.4	Classification of Conductive Hydrogels	16
4.5	Characteristics of Conductive Hydrogels	18
4.6	Developing an Enriched Composite Hydrogel For Wearable Displays	19
4.7	Results and Discussion	25
5	Part 3: Display Integration	26
5.1	Introduction to E-Ink Displays	26
5.2	Image Formation and Control in E-Ink Displays	27
5.3	Layered Architecture and Material Composition of E-Ink Displays	30
5.4	Developing a Novel Display Stack for Wearable E-Ink Displays	30
5.5	Results and Discussion	36
6	Conclusion	38
6.1	Summary	38
6.2	Future Explorations	38
A	AI Prompts	44
B	Code	45

List of Figures

1.1	E-Ink microcapsules containing one type of charged white pigment particles, while the darker pigment is dissolved in the suspension liquid. When an electric field is applied, the white pigment is attracted to the positive side, producing a light-coloured surface, while the opposite side shows the darker colour of the suspension liquid. (Figure from submitted paper by Wenda Zhao)	2
2.1	Illustration of current programmable inks used in HCI (top row: PrintScreen [23], Decochrom [22]; bottom row: Photochromic Canvas [13], TempTouch [26]).	4
3.1	Annex A of ISO 10993-1. A reference table categorising medical devices based on their type and duration of contact with human tissue, and corresponding biological endpoints.	8
4.1	A visual summary of the four key hydrogel classification categories. The central node represents hydrogels as a general material class, branching into four major categories: Source (natural vs synthetic), Preparation Method (homopolymeric, copolymeric, or interpenetrating networks), Crosslinking Type (physical or chemical), and Charge (cationic, anionic, neutral, or ampholytic). Informed by [8].	15
4.2	A visual summary of the two key conductive hydrogel classification frameworks. The central node represents conductive hydrogels as a material subclass, branching into two major frameworks: Conductive Material Type , which distinguishes between electronically conductive hydrogels (E-CHs)—including filler-type and conductive-polymer type—and ionically conductive hydrogels (I-CHs); and Network Structure , which categorises hydrogels based on their polymer architecture into single, double, or triple networks. Informed by [39, 44].	18
4.3	Photographs of a selection of synthesised hydrogel formulations. Images correspond to selected candidate gels from Tables 4.1, 4.2, 4.3, and 4.4. Each pair of images shows: (1) the hydrogel sample in isolation, and (2) the same sample placed on top of a sticky note with written text for a sense of the hydrogel's optical clarity. Shown are: (a) PVA, (b) PVA on sticky note, (c) [BMIM]TfO PAA Model, (d) [BMIM]TfO PAA Model on sticky note, (e) D.M Water/[BMIM]TfO PAA/PVP, (f) D.M Water/[BMIM]TfO PAA/PVP on sticky note, (g) D.M Water/[BMIM]TfO PAA/GE, (h) D.M Water/[BMIM]TfO PAA/GE on sticky note. Samples visibly differ in form, and optical clarity, reflecting their underlying material compositions, and stirring and UV curing conditions.	24
5.1	Cross-sectional diagram of an E-Ink microcapsule. An electric field applied between the top and bottom electrodes causes charged black and white pigment particles to migrate within the capsule, controlling the pixel's visible state. This electrophoretic mechanism enables bistable and reflective display behaviour.	27
5.2	Schematic optical trace showing particle movement and reflectivity changes in an electrophoretic display (EPD) during the driving waveform, showing time-based progression from the intended grayscale target (GT), to the achieved reflectivity (GT*), and the subsequent decline due to grayscale degeneration (GD*).	28
5.3	The general structure of a modified waveform for EPD (electrophoretic display) driving, showing the typical three-phase sequence: Erase (reset and shaking), Activate (particle mobilisation), and Display (grayscale rendering). This structure is designed to minimise visual artifacts such as ghosting, grayscale degradation, and DC imbalance.	29

5.4	Driving pulses for a multi-grayscale electrophoretic display using Pulse Amplitude Modulation (PAM) and Pulse Width Modulation (PWM). PAM varies voltage amplitude, while PWM varies pulse duration to control pigment particle displacement.	29
5.5	Cross-sectional diagram showing the layered architecture of an E-Ink display. The protective outer layer (PET), the transparent conductive layer (ITO), the electrophoretic imaging layer (E-INK + Adhesive) contains pigment-filled microcapsules embedded in a polymer matrix, bonded to the substrate via adhesive's, and the addressing layer (Backplane) contains the circuitry for pixel-level control.	30
5.6	Layered architecture of the BioPixel display prototype. Our design replaces the rigid PET and backplane of conventional E-Ink displays with two flexible ITO electrodes, and substitutes the conventional E-Ink microcapsule and adhesive layer with a biocompatible hydrogel-based electrophoretic layer ("E-Ink Gel"). The top ITO layer ("ITO Control") acts as the pixel-driving electrode, while the bottom ITO layer is intended to be removed in future iterations, allowing the wearer's skin, leveraging its natural conductivity, to function as the bottom electrode (contingent on successful biocompatibility validation of the E-Ink Gel).	31
5.7	Optical microscopy slide of the four evaluated E-Ink dispersions from 2023 laboratory stock, arranged from left to right: Red 1, White, Red 2, and Black.	32
5.8	Optical microscopy slides of PAA/GE/E-Ink hydrogel samples after Photopolymerisation under different exposure times, arranged from left to right Photo-1 to Photo-5.	34
5.9	Electronic architecture of the single-segment display prototype.	35
5.10	Verification of voltage polarity switching.	35
5.11	Electrophoretic switching test sequence. Panels (a)–(c) show three small hydrogel-E-Ink test samples (Photos 1–3) placed left to right on a single ITO substrate, captured before, during, and after application of up to ± 30 V. Panel (d) shows the final prototype fabricated using the same formulation and mixing conditions as Photo 3 (Mix-4 protocol), but cast in a larger mold. No visible colour switching was observed in any tests.	36

List of Tables

4.1	Formulations of polymer-based hydrogels using D.M Water as the primary solvent, with variations in the inclusion of PVA, GE, and PVP as structural and functional additives. PEGDA (0.5 g) and LAP (0.05 g) were used in all formulations.	22
4.2	Formulations of acrylic acid (AA)-based hydrogels incorporating the ionic liquid [BMIM]TfO, with optional inclusion of gelatin (GE) and PVP. D.M Water was used as a co-solvent. PEGDA (0.5 g) and LAP (0.05 g) were used in all formulations.	23
4.3	Magnetic stirring and UV curing conditions used for each hydrogel formulation. Conditions were adjusted to ensure homogenisation and consistent crosslinking across different compositions.	23
4.4	Hydrogel model characteristics with both measured electrical performance, and qualitatively assessed physical properties. Conductivity (mS) and resistance (MΩ) were measured using standard instrumentation, while transparency, mechanical robustness, and self-adhesion were evaluated through visual inspection and manual testing. “Yes” / “No” entries reflect whether each model qualitatively met our predefined criteria for those properties. The final “Conductive” column indicates whether the material demonstrated adequate conductivity for potential use in a wearable E-Ink display, with a “Yes” assigned to samples exhibiting a resistance of 1 MΩ or less.	23
5.1	Four mixing protocols used to incorporate E-Ink microcapsules into the hydrogel matrix. Each protocol varies mixing temperature, intensity, duration, and whether the E-Ink was added before or after base hydrogel mixing.	32
5.2	Photopolymerisation protocols.	33

Ethics Statement

- This project did not require ethical review, as determined by my supervisor
- This project fits within the scope of ethics application 0026, as reviewed by my supervisor
- An ethics application for this project was reviewed and approved by the faculty research ethics committee as application.

Notation and Acronyms

Acronyms

EPD	Electrophoretic Display
E-Ink	Electronic Ink (a type of EPD)
ITO	Indium Tin Oxide
TFT	Thin-Film Transistor
PET	Polyethylene Terephthalate
UV	Ultraviolet
PAM	Pulse Amplitude Modulation
PWM	Pulse Width Modulation
LUT	Lookup Table
CCA	Charge Control Agent
PVA	Polyvinyl Alcohol
PVP	Polyvinylpyrrolidone
PAA	Poly(acrylic acid)
GE	Gelatin
PEGDA	Poly(ethylene glycol) diacrylate
LAP	Lithium phenyl-2,4,6-trimethylbenzoylphosphinate
IL	Ionic Liquid
SN / DN / TN	Single-/Double-/Triple-Network (Hydrogel types)
[BMIM] TfO	1-butyl-3-methylimidazolium trifluoromethanesulfonate
NRU	Neutral Red Uptake (assay)
h-CLAT	Human Cell Line Activation Test
U-SENS™	In Vitro Sensitisation Assay
ISO	International Organisation for Standardisation
OECD	Organisation for Economic Co-operation and Development
PBS	Phosphate Buffered Saline
BSA	Bovine Serum Albumin
PI	Propidium Iodide
RPMI	Roswell Park Memorial Institute medium
SPDT	Single Pole Double Throw (electronic relay)
AFM	Atomic Force Microscopy
SEM	Scanning Electron Microscopy
TEM	Transmission Electron Microscopy
FTIR	Fourier Transform Infrared Spectroscopy
NMR	Nuclear Magnetic Resonance
DSC	Differential Scanning Calorimetry
TGA	Thermogravimetric Analysis
SAXS	Small-Angle X-ray Scattering
WAXS	Wide-Angle X-ray Scattering
DMA	Dynamic Mechanical Analysis
Tg	Glass Transition Temperature
IDT	Initial Decomposition Temperature

Notations

W_s	Weight of swollen hydrogel
W_d	Weight of dry hydrogel
R	Electrical resistance (Ohms)
σ	Electrical conductivity (Siemens per meter)
L	Distance between electrodes
A	Cross-sectional area of hydrogel
GF	Gauge Factor (sensitivity to strain)
M / mM	Molar / millimolar concentration (mol/L)
w/w	Weight by weight concentration
v/v	Volume by volume concentration
IC ₅₀	Half-maximal inhibitory concentration
GT	Grayscale Target
GT*	Achieved Grayscale
GD*	Grayscale after Degeneration
V	Voltage (Volts)
°C	Degrees Celsius
s	Seconds (time)
mW/cm ²	Power density (milliwatts per square centimetre)

Chapter 1

Introduction

1.1 Motivation

E-Ink displays, also known as electrophoretic or electronic paper displays, are designed to mimic the appearance of ink on paper. Traditional E-Ink displays are built in layers, typically consisting of a substrate layer (often plastic like PET), a transparent conductive layer, an adhesives layer containing the E-Ink itself, and a control backplane that contains the electronics for addressing each pixel [11]. Although Traditional E-Ink displays excel in energy efficiency, readability, and durability [11], their standard construction, from rigid or semi-rigid layers, incorporating E-Ink microcapsules containing hydrocarbon-based fluids, and multiple adhesives containing proprietary or potentially irritating chemicals, makes them unsuitable for direct skin contact or wearable use [19]. Consequently, E-Ink displays have remained largely limited to rigid formats like e-readers and electronic price tags, without evolving into more versatile forms such as wearable patches. This project specifically **envision applications where such programmable ink is embedded in wearables, in close contact with human skin, and potentially even used as digital tattoos.**

Indeed, E-Ink could serve as a valuable addition to the array of active materials utilised in the fabrication of digital devices. However, the production of E-Ink microcapsules remains a significant hurdle. This is primarily due to the intricate and resource-intensive nature of current manufacturing methods. Existing techniques demand specialised equipment and expertise in chemical and material engineering, making the process inaccessible to a wider audience. In addition, certain aspects of the production process involve handling potentially hazardous chemicals, which requires extensive training to mitigate associated risks. The complex procedures involved not only pose significant barriers to scalability and cost-effectiveness but also raise safety concerns, inhibiting the widespread adoption of E-Ink technology in practical applications. Consequently, despite its potential advantages, the integration of E-Ink into digital fabrication is limited.

Recently the scope for building a wearable E-Ink display has been opened by new research at the University of Bristol. Wenda Zhao, a collaborating PhD researcher on this project at the University of Bristol, my supervisor Anne Roudaut, and colleagues have developed a biocompatible E-Ink microcapsule. This work (currently under submission) addresses these challenges by introducing a novel method that simplifies the production of E-Ink microcapsules. Generally, E-Ink microcapsules contain two types of charged pigment particles—typically black and white—that move in opposite directions under an electric field. Their work introduces an alternative: the pipeline produces E-Ink microcapsules containing only a single type of charged white pigment particle, with the darker pigment dissolved in the suspension liquid. Upon application of an electric field, the white particles migrate toward the positive electrode, creating a light-coloured surface, while the opposite side reveals the darker hue of the suspension (Figure 1.1).

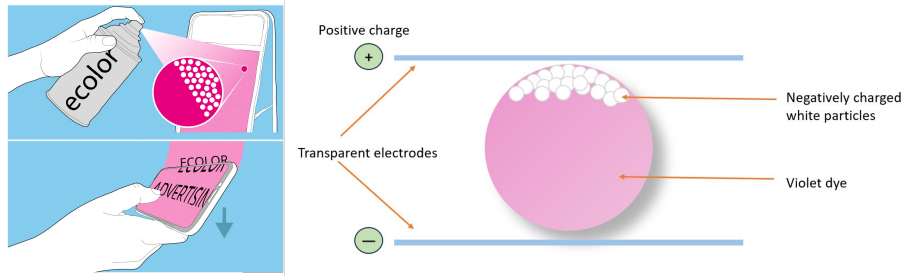


Figure 1.1: E-Ink microcapsules containing one type of charged white pigment particles, while the darker pigment is dissolved in the suspension liquid. When an electric field is applied, the white pigment is attracted to the positive side, producing a light-coloured surface, while the opposite side shows the darker colour of the suspension liquid. (Figure from submitted paper by Wenda Zhao)

However, as they clearly mention it in their paper, their work represents only a preliminary step toward the broader goal of accessible E-Ink display fabrication. Developing such ink involves complex challenges spanning chemical formulation and material integration. In particular several challenges remain to reach fully functional wearable displays:

- RQ1: Are the E-Ink microcapsules biocompatible in order to be used safely in close contact to human skin?
- RQ2: What types of biocompatible and conductive substrates they can be embedded in to replace traditional ITO?
- RQ3: How to integrate the ink the the conductive substrates into a functional device?

1.2 Contributions

Our general goal is to develop a functional 'digital tattoo'—a flexible, skin-adhering device similar to a temporary sticker—that enables continuous interaction or physiological monitoring without restricting movement [9]. But more precisely, we aim to answer the questions that are exposed above. This project is therefore atypical in its strong focus on materials, yet it fits within computer science research, as HCI increasingly pushes the boundaries of the field by integrating insights from other scientific disciplines [32]. Our contribution are the following:

- In Part 1 we reply to RQ1. We investigate the biocompatibility of the E-Ink microcapsules. The chapter reviews current standards for assessing biocompatibility, narrowing down to appropriate tests for our specific ink formulation, and presents the results of these tests. The findings suggest that the new E-Ink microcapsules are a promising candidate for safe epidermal integration.
- In Part 2 we reply to RQ2. We propose the use of hydrogel as a substrate for embedding E-Ink particles. We present related work in materials science that have introduced flexible electronic materials such as conductive hydrogels and ionogels. Building on these developments, we investigate the fabrication of conductive hydrogel substrate and report its performances. The finding shows that our hydrogel is highly transparent, mechanically robust, self-adhesive, and conductive.
- In Part 3 we reply to RQ3. We move on to integrating the hydrogel substrate and E-Ink micro-capsules into an initial prototype of an E-Ink display. This section outlines the basic operating principles of a standard E-Ink display setup and describes the modifications we made to adapt it for our custom materials.

Our work addresses the gap between recent advances in biocompatible electrophoretic materials, conductive flexible materials, and the development of a wearable E-Ink display. To this end this work documents the step-by-step effort to connect these two endpoints: by evaluating the biocompatibility of the newly developed microcapsules, developing a suitable hydrogel to replace the toxic adhesive layers in a traditional E-Ink display stack, and finally attempting to integrate these components into a cohesive, wearable E-Ink display.

1.3. TEAMWORK ASPECTS

By doing so our work contributes to the ongoing research at the University of Bristol and elsewhere into novel applications of electrophoretic (E-Ink) materials for flexible and wearable displays [11, 10] by (1) consolidating the required foundational knowledge on biocompatibility testing standards, electrophoretic display physics, and hydrogel design for researchers and developers working towards creating a wearable E-Ink display, (2) designing and synthesising a new conductive hydrogel specifically designed for wearable displays, combining mechanical robustness, high optical transparency, high conductivity, and implicit biocompatibility (the individual components are biocompatible), and (3) attempting to prototype a wearable E-Ink display that integrates the biocompatible E-Ink microcapsules into our conductive hydrogel to create a wearable E-Ink display.

Although a fully functional wearable E-Ink display was not achieved in the scope of this project (the final tested samples exhibited no visible colour switching within the applied voltage range), this work makes important contributions toward the development of a wearable E-Ink display. It lays critical groundwork for future researchers and developers by consolidating the necessary technical knowledge, designing a novel mechanically robust, highly conductive, and transparent hydrogel for use in wearable displays, and identifying key material limitations in the current generation of biocompatible E-Ink microcapsules, their fragility and poor UV stability, that must be addressed before a working E-Ink display can be realised.

1.3 Teamwork Aspects

Throughout this report, I use the pronoun "we" to reflect the collaborative nature of the work. This project was not a typical student assignment; rather, I was fully embedded in a research team working to advance knowledge on a novel E-Ink microcapsule formulation. As such, the use of "we" acknowledges the collective effort behind the research.

To clarify my contributions: in Part 1 (biocompatibility), I collaborated with the team and was primarily responsible for better understanding the norms and standard around bio-compatibility testing, which in turns helped to determine the appropriate biocompatibility tests for the new ink. Although I did not handle the chemical myself for the lab tests, due to training requirements, I was involved throughout the entire process. In Part 2 (hydrogel substrate), I led the work independently. I proposed the idea of using hydrogel as a substrate and drove the design and experimentation process. The team supported me by helping procure chemicals, and I also engaged in collaborative brainstorming with the team during the iterative development of the hydrogel formulation. In Part 3 (display integration), I led the integration of the E-Ink microcapsules and hydrogel substrate into an early display prototype. While I regularly exchanged feedback with the team, the development and execution of this section were primarily my responsibility.

1.4 Report Organisation

This report is made of 6 chapters.

- Chapter 1 introduces the motivations of this work alongside the contributions.
- Chapter 2 discusses related work that is specific to the fabrication of interactive devices using programmable ink. This chapter is relatively small given that the subsequent chapters contain literature of respective topics.
- Chapter 3, 4 and 5 present respectively the part 1 (bio-compatibility), part 2 (hydrogel substrate) and part 3 (device integration).
- Chapter 6 concludes this work and present avenues for future work.

Chapter 2

Related Work on programmable ink fabrication

In this section, we discuss related work that investigate the usage of programmable ink to create interactive displays. We explain the structure and composition of E-Ink microcapsules. We also discuss the use of hydrogels.

2.1 Programme Inks in HCI

Several programmable ink have been explore as shown in Figure 2.1.

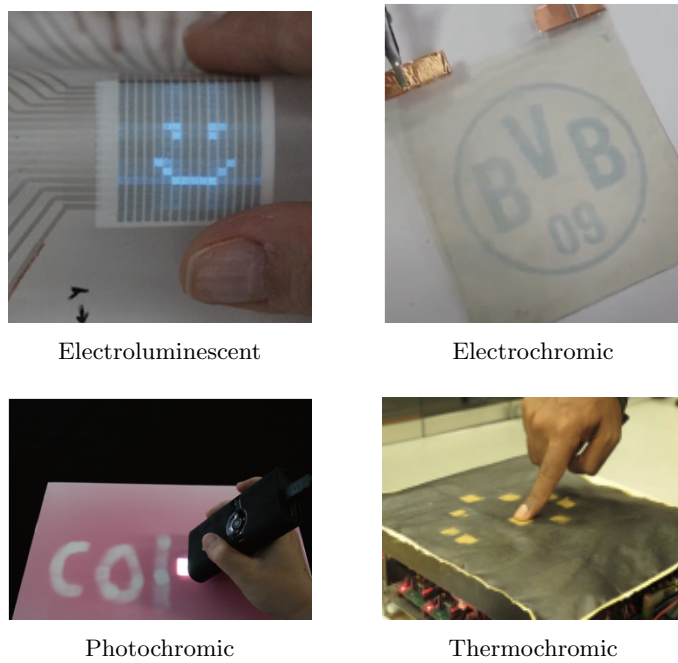


Figure 2.1: Illustration of current programmable inks used in HCI (top row: PrintScreen [23], Decochrom [22]; bottom row: Photochromic Canvas [13], TempTouch [26]).

Electroluminescent (EL) materials have been widely investigated in HCI. For instance, PrintScreen [23] introduced fabrication techniques that make EL-based display elements accessible to non-experts, enabling both segmented and pixel-based designs. The Strechis project [38] extended this concept to deformable, stretchable interfaces. More recently, approaches like ProtoSpray and Sprayable User Interfaces [12, 37] have demonstrated how spraying combinations of conductive and EL inks can turn physical objects into interactive display surfaces.

Electrochromic materials have also been the focus of extensive research. The Decochrom project [6] has led much of this work, producing a range of HCI publications that explore the interactive potential of these inks. Notable contributions include those by Löchtefeld et al. [21], Müller et al. [22], and Jensen et al. [16], who developed diverse fabrication approaches and applications for electrochromic displays.

Photochromic materials change colour in response to light. They introduced to interactive fabrication in PhotoChromic Canvas by Hashida et al. [13]. Subsequent innovations such as ColorMod [30] enabled reprogrammable full-color objects via 3D printing. PhotoChromeleon [17] achieved finer color control through blended photochromic inks, while ChromoUpdate [36] focused on improving refresh speed. In a parallel direction, ChromoPrint [31] explored embedding photochromic dyes into resin-based 3D prints.

Thermochromic materials, which respond to temperature changes, have also found applications in HCI. Projects like TempTouch [26] and AmbiKraf [27] used embedded heating elements to activate color shifts. More recently, Thermotion [43] advanced this concept with 3D-printed thermal channels, enabling quicker and more localised color transitions.

Electrophoretic materials, such as those used in E Ink displays, remain relatively under explored in HCI. One early effort by Sweeney et al. [33] proposed an architecture for digital displays built from soft materials like textiles and plastic films, where each pixel is capable of both sensing and display output. Their prototypes highlighted the feasibility of this vision, although the electrophoretic layer they used was limited to commercially available sheet formats that had to be manually cut to match the device's geometry. Other researchers have also leveraged commercial E Ink screens to explore novel applications. For example, AlterWear [7] demonstrated how E Ink panels can be incorporated into wearable systems using stencil patterns to explore new interactive form factors. More recently, Fabricatink by Hanton et al. [11] explored the upcycling of E Ink panels from discarded e-readers for use in free-form display fabrication. Their work underscores the significant barriers to broader adoption: producing electrophoretic microcapsules from scratch is highly challenging, and accessing commercial sources is complicated by intellectual property restrictions. Moreover, reusing existing screens involves delicate processes—chemical treatments or physical separation steps can easily damage the active material, especially during disassembly or cutting.

2.2 E-Ink Microcapsules

E-Ink microcapsules are composed of three primary components: a polymer shell, a dielectric fluid, and charged pigment particles [11]. The encapsulation shell functions as a barrier that contains the dielectric fluid and pigment particles while providing mechanical stability and optical transparency. This shell must be chemically inert, flexible, and resistant to breakage to ensure the longevity of the display. Manufacturers often use synthetic polymers such as polyurethane, polyamine, polysulfones, polyethylene acid, and cellulose derivatives [29].

The dielectric fluid within the microcapsules serves as a low-conductivity medium that enables electrophoretic movement while maintaining particle suspension. It must be chemically stable, non-volatile, and have a refractive index closely matched to the pigment particles to optimise visual contrast. Manufacturers often use isoparaffinic hydrocarbons such as Isopar-G and Isopar-M, or halogenated hydrocarbons like perfluorohexane or fluorinated oils, typically combined with *CCAs* (charge controlling agents) and other additives [4].

The charged pigment particles within the microcapsules are responsible for the display's optical switching behaviour. These particles are typically nano-sized (10-500 nm). They must be able to exhibit strong, opposing electrical charges while remaining suspended in the dielectric fluid. Manufacturers often use titanium dioxide (TiO_2) for white and positively charged carbon black for black [11].

A widely used method for fabricating microcapsules is complex coacervation, a process in which two oppositely charged polymers interact to form a thin, protective shell around liquid droplets. When these polymers are mixed under the right environmental conditions, such as specific pH and temperature, they separate out of the solution and coalesce around suspended particles or liquid cores. This process is driven primarily by electrostatic attraction between the polymers, often aided by controlled cooling to

2.3. USE OF HYDROGEL

solidify the shell. The final shell structure can be further stabilised by introducing a crosslinking agent, which chemically binds the polymer chains, improving the mechanical strength and durability of the microcapsules [34].

2.3 Use of Hydrogel

Conductive gels, including hydrogels and ionogels, have been widely explored in a wide range of work for wearable electronics. These studies predominantly use biopolymer or synthetic polymer matrices swollen with water (for hydrogels) or ionic liquids (for ionogels), and incorporate conductive fillers and ionic modifiers to tailor mechanical flexibility and electrochemical performance to the specific requirements of a target device. The closest work to our conductive hydrogel, Yuan et al.[44] demonstrate a highly stretchable, transparent, and self-adhesive ionic conductor fabricated by photopolymerising acrylic acid (AA) in the ionic liquid [BMIM]TfO. This work focuses on developing a highly stretchable, transparent, and self-adhesive PAA ion gel for wearable strain and temperature sensing. BioPixel modifies this system for a different application, a wearable E-Ink display that requires a more implicitly biocompatible hydrogel.

Other work incorporated into BioPixel’s conductive hydrogel design includes, Xu et al.[39], which reviews PVA-based conductive hydrogels using filler materials and tunable network structures to create strain-sensitive soft sensors, Yi et al.[41] which explore a physically cross-linked PVA/PVP hydrogel with strain responsiveness and humidity sensitivity through a freeze–thaw process, and Wang et al.[35] which investigates gelatin hydrogels reinforced with carbon nanomaterials, conducting polymers, and metallic nanostructures for antibacterial, self-healing, and wearable sensor applications.

2.4 Summary

To our knowledge, no wearable E-Ink display has been fabricated by dispersing E-Ink microcapsules as functional additives within a conductive hydrogel. There exists work that has opened the application scope for wearable, flexible displays, Olberding et al. [24] introduces ultra-thin, flexible electroluminescent displays that can be printed on materials like paper, PET, and leather, and Wessely et al. [38] introduces ultra-thin and stretchable electroluminescent displays.

More recent work has identified E-Ink as a promising material for developing flexible, wearable displays, Hanton et al. [11] introduces E-Ink as a material for fabricating flexible, low-power displays by airbrushing upcycled E-Ink onto paper, and Hanton et al. [10] highlights bistable materials like E-Ink as particularly promising for wearable displays due to their high contrast, flexibility, and ultra-low power consumption, traits that make them ideal for skin-mounted and energy-constrained applications.

Chapter 3

Part 1: Biocompatibility

In this chapter, we begin by introducing the concept of biocompatibility, followed by an overview of standard testing protocols as defined by the ISO 10993 series. Emphasis is placed on the ISO 10993 series because it represents the most widely recognised and internationally harmonised framework for biocompatibility testing, and ultimately forms the benchmark against which all biocompatibility testing is assessed [28]. A clear understanding of these standards is essential before initiating any evaluation process. We then describe how these guidelines are applied in practice, focusing specifically on cytotoxicity and sensitisation testing, as they are the most critical first-line evaluations in testing the biocompatibility of any material, providing early, high-confidence indicators of whether a material is biocompatible [18]. And finally, we present the biocompatibility tests conducted on the E-Ink formulation developed in Bristol, including the methodology and results.

3.1 Introduction to Biocompatibility

Biocompatibility can be defined as:

“the ability of a medical device or material to perform with an appropriate host response in a specific application [1].”

The testing of biocompatibility is set out in guideline documents issued by various national and international standards agencies ”American Society for Testing and Materials, Health Industry Manufacturers Association, American Dental Association, Food and Drug Administration in the USA, British Standards Institution in the UK, Association Francaise de Normalization in France, Deutsches Institut fur Normung in Germany, Ente Nazionale Italian di Unificazione in Italy, International Organization for Standardisation, etc.” [28].

These guidelines are now consolidated in ‘Biological Testing of Medical Devices–Part 1: Guidance on Selection of Tests’ (ISO 10933-1) which integrates all the national and international documents into one structured approach for the biological evaluation of medical devices [1].

3.2 Understanding the ISO 10993 Series

ISO 10993 aims to protect humans from the potential biological risks associated with the use of medical devices. To achieve this, ISO 10993-1 outlines a set of general principles for the biological evaluation of medical devices within a risk management structure. These principles combine the review and evaluation of existing data from all sources, and where necessary, the identification and application of additional tests to evaluate the biological response to each medical device, appropriate to its safety in use [1].

In the context of ISO 10993, the term “medical device” encompasses a broad spectrum of devices, ranging from those composed of a single material, potentially existing in multiple physical forms, to complex devices made up of multiple components, each consisting of different materials [1].

Given this variability, ISO 10993 does not define medical devices by specific types but categorises medical devices based on their intended contact with human tissues, grouping them into surface-contacting devices e.g., ”electrodes, compression bandages, contact lenses, urinary catheters” [28], external-communicating

3.3. IMPLEMENTING THE ISO 10993 SERIES

devices e.g., "dental cements, arthroscopes, intravascular catheters, dialysis tubing" [28], and implantable devices e.g., "hip and knee prostheses, pacemakers, artificial tendons, heart valves" [28]. Further grouping is done based on the duration of the device's contact with human tissue: limited exposure (< 24 h), prolonged exposure (> 24h and < 30days), and permanent contact (> 30days) [1].

These device classifications help form a reference table, Annex A of ISO-10993, See Figure 3.1, which can assist professionals—qualified through training and experience—in identifying the specific biological *endpoints* (effects) that must be evaluated to ensure the biocompatibility of a medical device. In this way rather than prescribing fixed test methods, or pass/fail criteria, ISO 10993 provides a flexible framework that allows experts to select appropriate evaluation strategies based on the scientific evidence that are tailored to each device's specific use, while maintaining rigorous safety standards [1].

Medical device categorization by		Biological effect									
Category	Contact	nature of body contact (see 5.2)	contact duration (see 5.3)	Cytotoxicity	Sensitization	Irritation or intracutaneous reactivity	Systemic toxicity (acute)	Subchronic toxicity (subacute toxicity)	Genotoxicity	Implantation	Haemocompatibility
			A – limited (≤ 24 h)	X ^a	X	X					
			B – prolonged <td>X</td> <td>X</td> <td>X</td> <td></td> <td></td> <td></td> <td></td> <td></td>	X	X	X					
			C – permanent (> 30 d)	X	X	X					
Surface device	Skin	A	X ^a	X	X						
		B	X	X	X						
		C	X	X	X						
	Mucosal membrane	A	X	X	X						
		B	X	X	X						
		C	X	X	X			X	X		
	Breached or compromised surface	A	X	X	X						
		B	X	X	X						
		C	X	X	X			X	X		
External communicating device	Blood path, indirect	A	X	X	X	X					X
		B	X	X	X	X					X
		C	X	X		X	X	X	X		X
	Tissue/bone/dentin	A	X	X	X						
		B	X	X	X	X	X	X	X	X	
		C	X	X	X	X	X	X	X	X	
	Circulating blood	A	X	X	X	X					X
		B	X	X	X	X	X	X	X	X	X
		C	X	X	X	X	X	X	X	X	X
Implant device	Tissue/bone	A	X	X	X						
		B	X	X	X	X	X	X	X	X	
		C	X	X	X	X	X	X	X	X	
	Blood	A	X	X	X	X	X	X		X	X
		B	X	X	X	X	X	X	X	X	X
		C	X	X	X	X	X	X	X	X	X

^a The crosses indicate data endpoints that can be necessary for a biological safety evaluation, based on a risk analysis. Where existing data are adequate, additional testing is not required.

Figure 3.1: Annex A of ISO 10993-1. A reference table categorising medical devices based on their type and duration of contact with human tissue, and corresponding biological endpoints.

3.3 Implementing the ISO 10993 Series

The ISO 10993 series defines tests for assessing biological endpoints, with cytotoxicity (ISO 10993-5:2009), skin sensitisation (ISO 10993-10:2010), and irritation (ISO 10993-10:2010) historically forming the foundation of biocompatibility evaluation—commonly known as "The Big Three" [18]. Previously combined under ISO 10993-10:2010, sensitisation and irritation are now addressed separately in ISO 10993-10:2021 and ISO 10993-23:2021. This revision places greater emphasis on cytotoxicity and sensitisation as core components of initial biocompatibility assessment while recognising irritation as a distinct evaluation pathway.

3.4. BIOCOMPATIBILITY TESTING OF THE NOVEL E-INK MICROCAPSULE

Cytotoxicity testing is an *in vitro* (outside a living organism) test, used to assess a device's impact on living cells. Using ISO-approved cell lines exposed to *extracts* (solutions obtained by immersing device components in solvents such as saline, vegetable oil, or cell culture medium) of the device or its materials, and typically employing quantitative methods such as MTT, XTT, or Neutral Red Uptake, a material is classified as non-cytotoxic, mildly cytotoxic, moderately cytotoxic, or highly cytotoxic, based on the percentage of *viable cells* (cells that have survived and can proliferate) at least 24 hours after exposure. Any cytotoxic effect can be of concern. However, generally, a $\geq 70\%$ cell viability is considered favourable, particularly when testing neat extracts [18].

Sensitisation testing, while historically an *in vivo* (inside a living organism) test, is now typically an *in vitro* test, used to assess a device's potential to trigger an immune response [2]. Using ISO-approved immune-relevant cells exposed to extracts of the device or its materials, and typically employing quantitative methods such as h-CLAT or U-SENS™, a material is classified as a sensitiser or non-sensitiser based on surface marker expression (detection of immune response-related proteins) at a set amount of time after initial exposure [3]. For h-CLAT and U-SENS™, a $\geq 150\%$ increase in surface marker expression compared to the control classifies a material as a sensitiser [25]. However, since no single test provides a definitive classification, ISO 10993-10:2021 recommends integrating multiple methods, found in Annex C of ISO 10993-10:2021.

3.4 Biocompatibility Testing of the Novel E-Ink Microcapsule

Biocompatibility testing of the new E-Ink Microcapsule is intended to determine whether the microcapsules can enable an E-Ink display in which human skin, due to its inherent conductivity, can function as the displays bottom electrode, eliminating the need for additional substrate layers.

The newly developed biocompatible E-Ink microcapsule comprises polymer-coated TiO₂ nanoparticles suspended in a dielectric solution containing hexyl salicylate, tetrachloroethylene, and Nile red dye. These components are encapsulated using a complex coacervation method with gelatin B and gum arabic as the shell materials. In this process, gelatin and gum arabic—chosen for their biocompatibility, transparency, and safety—are dissolved separately in water to form colloidal solutions. The gum arabic solution is first mixed into the pigment suspension, followed by the gradual addition of the gelatin solution. The pH of the mixture is then adjusted to approximately 4.0 using acetic acid, which triggers complex coacervation and leads to the formation of a polymer shell around the pigment-containing droplets. Cooling the mixture to 5°C facilitates shell solidification. To further stabilise the microcapsules, glyceraldehyde, a low-toxicity crosslinker—was added to chemically link the gelatin and gum arabic polymers. The resulting microcapsules were washed and dried, yielding stable, functional E-Ink particles suitable for integration into display system.

Note that concentrations of chemical solutions are expressed using standard scientific units. The terms **w/w** (weight by weight) and **v/v** (volume by volume) refer to how the proportion of one substance is measured relative to the total weight or volume of the solution, respectively. For example, a 20% w/w solution contains 20 grams of solute per 100 grams of total mixture, while a 30% v/v solution contains 30 millilitres of solute per 100 millilitres of total solution. Additionally, molar concentrations are reported in M (Molar) and mM (millimolar) units. 1 M (Molar) represents one mole of a substance per litre of solution. The mM unit is a submultiple, with 1 mM equating to 1/1000th of a mole per litre (i.e., 0.001 M). For example, a 0.1 M solution of dinitrochlorobenzene refers to 0.1 moles of the compound dissolved per litre of solvent.

3.4.1 Skin Sensitisation Testing via THP-1 Cell Line Activation Test (h-CLAT)

To evaluate whether the E-Ink microcapsule formulation induces skin sensitisation, we performed the human Cell Line Activation Test (h-CLAT), an established *in vitro* assay that measures the expression of co-stimulatory molecules CD86 and CD54 in THP-1 cells following exposure to the test material.

3.4. BIOCOMPATIBILITY TESTING OF THE NOVEL E-INK MICROCAPSULE

Materials and Methods

A. Cells and Medium

THP-1 cells were seeded at a density of 1×10^6 cells/mL in 48-well plates, with 1000 μL per well. Cells were maintained in RPMI (Roswell Park Memorial Institute medium) 1640 medium supplemented with 0.05 mM 2-mercaptoethanol and 10% fetal bovine serum. To ensure cell viability and appropriate seeding density, cultures were monitored every two days using an automated cell counter, and cell concentrations were adjusted as needed.

B. Chemical Treatment of THP-1

The whole assay consists the following group: 1. Positive control. Cells exposed to 0.1M dinitrochlorobenzene; The positive group causes an 100 % sensitisation response. 2. (Testing group) six different concentrations of the sensitising agent (E-Ink microcapsules): 0%, 5%, 10%, 20%, 30%, and 50% 3. (Testing group) Empty microcapsule, Gelatin and Gum Arabic (GE-GA) based, 20% w/w 4. (Testing group) Nanoparticles (TiO_2), 20% w/w 5. (Testing group) Mixture of Gelatin and Gum Arabic, 0.1M 6. (Testing group) Tetrachloroethylene, 30 % v/v Negative control, cells seeding in equivalent amount of PBS

After seeding, THP-1 cells were exposed to six different concentrations of the sensitising agent (E-Ink microcapsules): 0%, 5%, 10%, 20%, 30%, and 50% for 24 hours at 37°C in a humidified incubator with 5% CO_2 . Each condition was prepared in triplicate, alongside both positive and negative control wells, resulting in a total of 24 wells.

C. Flow cytometric analysis

Following 24 hours of treatment, THP-1 cells were harvested by centrifugation. Centrifugation conditions were optimised based on the size of the nanoparticles. The cells were then washed twice with PBS (Phosphate Buffered Saline) containing 1% BSA (Bovine Serum Albumin) and seeded into 96-well round-bottom plates at a density of 1×10^5 cells per well in a maximum volume of 250 μL . For each condition, two wells were prepared: one for antibody staining and one for isotype control staining.

An optional Fc receptor blocking step was performed by incubating cells on ice for 20 minutes. Cells were then centrifuged at 400 g for 3 minutes at room temperature, washed once with PBSAG (PBS with 0.5% BSA and 0.01% sodium azide), and centrifuged again under the same conditions.

Staining was performed using anti-CD86 PE and anti-CD54 APC antibodies, along with IgG1 PE and IgG1 APC isotype controls, all diluted 1:50 in PBS containing 1% BSA. A volume of 20 μL of antibody solution was added to each well, mixed thoroughly, and incubated for 30 minutes at 4°C in the dark.

After staining, 200 μL of PBSAG was added to each well, followed by centrifugation at 400 g for 3 minutes. Cells were then resuspended in 100 μL of PBSAG for flow cytometry. PI (Propidium Iodide) (Miltenyi, 130-093-233) was added automatically at a 1:100 dilution immediately before acquisition to exclude non-viable cells.

Samples were acquired using a flow cytometer, and a minimum of 10,000 live events per condition were recorded. Compensation panels were prepared if required. Uptake volume was calculated as the total sample volume minus the dead volume (approximately 30 μL).

3.4.2 Cytotoxicity Testing Using the Neutral Red Uptake (NRU) Assay

To assess whether the E-Ink microcapsule formulation exhibits cytotoxic effects on skin cells, we conducted the Neutral Red Uptake (NRU) assay, an established *in vitro* test that measures cell viability based on lysosomal uptake of the neutral red dye following exposure to the test material.

Materials and Methods

A. Cells and Medium

3.5. RESULTS AND DISCUSSION

Normal human epidermal keratinocytes (NHEK) were cultured in serum-free Keratinocyte Growth Medium 2 (PromoCell) supplemented with 0.004 ml/ml Bovine Pituitary Extract, 0.125 ng/ml Epidermal Growth Factor (recombinant human), 5 µg/ml Insulin (recombinant human), 0.33 µg/ml Hydrocortisone, 0.39 µg/ml Epinephrine, 10 µg/ml Transferrin (recombinant human) and 0.06 mM CaCl₂. Cells were maintained at 37°C in a humidified incubator with 5% CO₂. Prior to seeding, cell viability was confirmed to be ≥95% using 0.4% trypan blue exclusion.

Cells were detached using 0.05% trypsin–0.02% EDTA and resuspended in complete medium. A uniform single-cell suspension was prepared and diluted to a final density of 5 × 10⁴ cells/mL. A volume of 200 µL was seeded into the inner wells of a 96-well plate, while peripheral wells were filled with PBS to minimise edge effects. Plates were incubated under standard conditions until a half-confluent monolayer formed.

B. Chemical Treatment

All test formulations were prepared under sterile conditions immediately prior to use. If necessary, solutions were passed through a 0.22 µm filter to ensure sterility. Treatments were applied in increasing concentrations (e.g., 0.01 to 100 µg/mL) to columns C4–C11. Columns C1 and C12 served as blank controls (medium only), C2 as an untreated cell control, and C3 as a solvent control when applicable. Treatment medium with reduced or no serum content was used to minimise protein binding interactions. Cells were incubated for 24 hours at 37°C in 5% CO₂.

C. Neutral Red Uptake Assay

A neutral red stock solution (4 mg/mL) was prepared by dissolving 40 mg of dye in 10 mL of PBS. The solution was stored at room temperature (20–30°C) for up to two months, protected from light. The working solution (40 µg/mL) was prepared the day before use by diluting the stock 1:100 in culture medium. Plates containing the working solution were incubated overnight at 37°C before application.

Prior to use, the neutral red working solution was centrifuged at 600 g for 10 minutes to remove any precipitated dye. After the 24-hour treatment period, cell medium was aspirated and, if necessary, cells were gently washed with 150 µL of PBS to remove precipitate. Then, 100 µL of neutral red medium was added to each well, and plates were incubated for 2 hours under standard conditions. If cells had low density or metabolic activity, this time could be extended up to 4 hours.

Plates were visually inspected under a microscope to assess dye uptake and check for precipitation. Following incubation, the medium was removed, and cells were washed with PBS. A volume of 150 µL of neutral red destain solution (50% ethanol, 49% deionised water, 1% glacial acetic acid) was added to each well. Plates were shaken vigorously for at least 10 minutes until the dye was completely extracted and a homogeneous solution was achieved.

Absorbance was measured at 540 nm using a microplate reader. Blanks containing only medium (no cells) were used as the reference. Data were saved in an appropriate file format for analysis. Dose–response curves were plotted and IC₅₀ values were calculated where possible. Experiments were repeated independently at least three times using a range of concentrations covering 0–100% inhibition.

3.5 Results and Discussion

Cell viability results from the Neutral Red Uptake (NRU) assay indicate that the E-Ink microcapsule formulation is not cytotoxic within the tested range. At the highest concentration tested (1 µg/µL), the formulation maintained 84.6% viability in NHEK cells. Lower concentrations showed higher viabilities, with 93.1% at 0.1 µg/µL and 102.6% at 0.01 µg/µL. As none of these concentrations reduced viability below 50%, however no IC₅₀ could be determined at this stage.

Component-specific testing at 1 µg/µL also indicated low cytotoxicity: TiO₂ nanoparticles resulted in 94.9% viability, hexyl salicylate 99.3%, and tetrachloroethylene (TCE) 96.3%. These results suggest that both the full microcapsule formulation and its internal components are non-toxic under the conditions

3.5. RESULTS AND DISCUSSION

tested.

These early results support the feasibility of using the microcapsule formulation in skin-contact applications such as wearable E-Ink displays. The absence of sensitisation and significant cytotoxicity is encouraging for designs that rely on direct skin contact. While further testing is needed, the formulation appears to be a promising candidate for safe epidermal integration.

Chapter 4

Part 2: Hydrogels

In this chapter, we introduce hydrogels and provide a classification of their types, followed by a discussion on their key properties and characterisation methods. Emphasis is placed on classification and characterisation as they form the critical foundation for any hydrogel research or design process. Given the breadth of existing literature and material diversity, identifying the appropriate hydrogel class and property profile based on application-specific requirements is essential before designing any hydrogel. We then focus on conductive hydrogels, detailing their specific characteristics and relevance to electronic applications, again framing classification and characterisation as a prerequisite to informed hydrogel design. Finally, we present the development of our custom hydrogel substrate for embedding E-Ink microcapsules, along with an evaluation of its fabrication process.

4.1 Introduction to Hydrogels

Hydrogels are soft, and flexible water-based gels that combine solid-like structural integrity with liquid-like permeability. On a molecular level hydrogels are made of three-dimensional networks of hydrophilic polymers capable of absorbing significant amounts of water ($> 10\%$ by definition). Hydrogels are synthesised by chemically or physically crosslinking natural or synthetic polymers into stable, interconnected matrices [8].

The crosslinked polymer structure of hydrogels enables them to absorb and retain large quantities of water while remaining insoluble. The absorbed water plasticises the polymer network, allowing the material to exhibit liquid characteristics at the molecular level and thus demonstrating a viscoelastic (both elastic and viscous) behaviour. At the same time, the crosslinked scaffold prevents the water from leaking out, allowing hydrogels to maintain a fixed volume and shape [39].

Due to their water-containing property, hydrogels are generally considered biocompatible, environmentally friendly, and biodegradable [8]. The characteristics of hydrogels can be further creatively adjusted by modifying their polymer composition, crosslinking density, fabrication method, and incorporating functional additives, making them highly adaptable to diverse applications requiring a soft, and flexible solid-like material [8, 39, 41, 35].

4.2 Classifying Hydrogels

While hydrogels have been widely studied, there is currently no internationally standardised system for their classification or characterisation. Different studies and reviews classify hydrogels according to a variety of criteria, and often emphasise different characteristics depending on their application focus. As a result, the terminology and grouping of hydrogels can vary considerably between publications. In this section, we aim to distil the essential aspects of hydrogels into our own simplified and coherent classification and characterisation scheme to facilitate clearer understanding and comparison.

Previous papers do not provide a universally standardised classification system for hydrogels. However there is broad consensus around four key categories. Hydrogels are typically classified based on their **source**, **preparation** method, **cross-linking** method, and the **charge** of their polymeric chains [8].

4.2. CLASSIFYING HYDROGELS

See Figure 4.1 for a visual summary outlining these four classification categories and their respective subcategories, informed by [8].

- **Source:** Hydrogels are classified based on their source as either **natural** or **synthetic**. Natural hydrogels are derived from natural biomass sources. Natural hydrogels are typically prepared using polysaccharides (e.g., alginate, chitosan, cellulose) or proteins (e.g., collagen, gelatin). Synthetic hydrogels are engineered from well-defined monomers or polymers. Synthetic hydrogels are typically prepared using polyethylene glycol (PEG), polyvinyl alcohol (PVA), or polyacrylamide (PAM)[8, 39].
- **Preparation Method:** Hydrogels are classified by preparation method into **homopolymeric**, **copolymeric**, and **interpenetrating polymer network** (IPN) types. Homopolymeric hydrogels consist of a single polymer with identical repeating monomers, while copolymeric hydrogels incorporate multiple monomers (at least one hydrophilic) arranged in block, random, or alternating configurations. IPN hydrogels involve two distinct crosslinked polymers within a shared network, whereas semi-IPNs contain one crosslinked and one linear polymer [8].
- **Crosslinking Method:** Hydrogels are classified based on cross-linking methods, primarily **physical** or **chemical**. Physical cross-linking employs temporary junctions, such as physical entanglement of the polymer chains and non-covalent forces (e.g., ionic forces, hydrogen bonds, and hydrophobic interactions) through methods such as freeze-thawing. Chemical cross-linking forms stronger covalent linkages, including permanent and dynamic covalent cross-links through methods such as photo-, redox-, thermal-, or radiation-initiated free-radical polymerisation, enzyme-enabled reactions etc [8].
- **Charge of Polymeric Chain:** Hydrogels are classified by the charge of their polymeric chains into **anionic**, **cationic**, **neutral**, or **ampholytic types**. Anionic hydrogels contain negatively charged groups (e.g., carboxylate or sulfate groups), while cationic hydrogels have positively charged groups (e.g., amine groups). Neutral hydrogels lack a net charge, relying on non-ionic interactions for stability. Ampholytic hydrogels contain both positive and negative charges [8, 39].

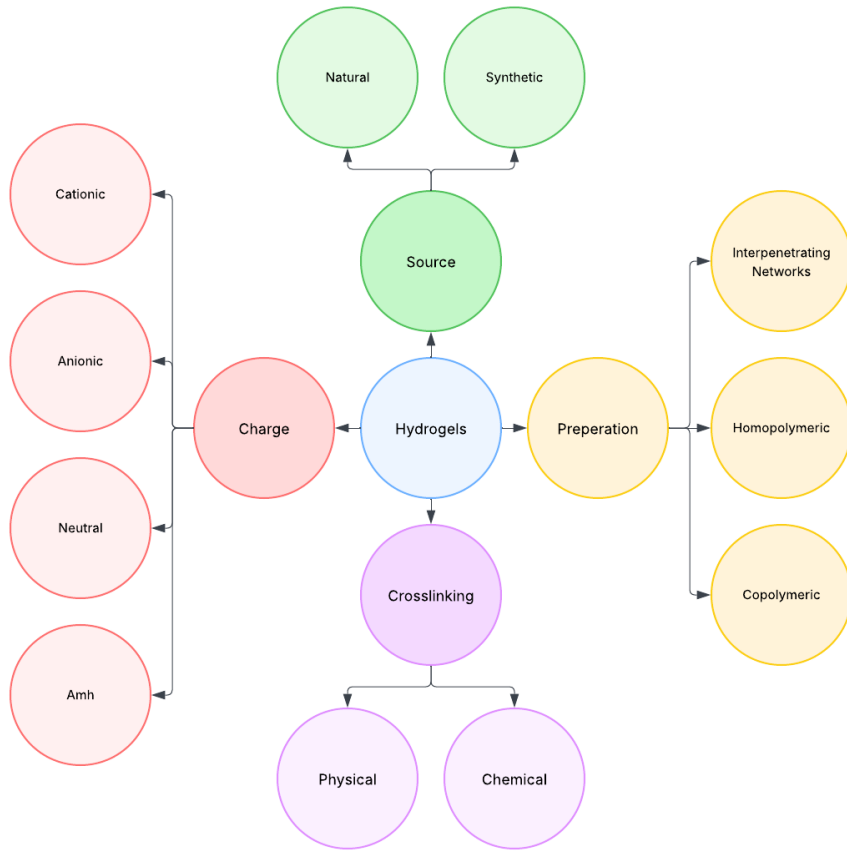


Figure 4.1: A visual summary of the four key hydrogel classification categories. The central node represents hydrogels as a general material class, branching into four major categories: **Source** (natural vs synthetic), **Preparation Method** (homopolymeric, copolymeric, or interpenetrating networks), **Crosslinking Type** (physical or chemical), and **Charge** (cationic, anionic, neutral, or ampholytic). Informed by [8].

4.3 Characterisation of Hydrogels

Hydrogels possess several key characteristics that are essential for understanding their design, functionality, and application potential. These include **chemical structure**, **swelling behaviour**, **morphology**, **mechanical properties**, **texture**, **thermal properties**, and **biocompatibility** [8].

4.3.1 Chemical Structure

Chemical structure describes the arrangement of functional groups and molecular organisation within the hydrogel network. It is measured using spectroscopic techniques such as FTIR, Raman, NMR, EDX, XRD, and EDS, which identify specific chemical bonds and functional groups [8]. Understanding the chemical structure of a hydrogel allows us to design the hydrogel with specific functionalities and predict its performance in various applications.

4.3.2 Swelling

Swelling describes the ability of hydrogels to absorb and retain water or biological fluids. It is measured by determining the equilibrium swelling ratio, calculated as the ratio of the weight of the swollen hydrogel to the weight of the dry hydrogel.

$$\text{Swelling} = \frac{W_d}{W_s - W_d}$$

4.4. CLASSIFICATION OF CONDUCTIVE HYDROGELS

where W_s is the weight of the swollen hydrogel and W_d is the weight of the dry hydrogel [8]. Understanding the swelling of a hydrogel allows us to determine the suitability of the hydrogel for biomedical and environmental use.

4.3.3 Mechanical Robustness

Mechanical robustness describe how hydrogels respond to applied forces such as viscoelasticity, tensile strength, compressive modulus, and elasticity. It is measured using techniques like dynamic mechanical analysis (DMA) and tensile testing [8]. Understanding the mechanical properties of a hydrogel allows us to determine the hydrogel's durability, flexibility, and suitability for load-bearing or wearable applications.

4.3.4 Morphology

Morphology describes the physical structure of hydrogels, particularly their porous architecture and network arrangement. It is measured using microscopy techniques such as SEM, TEM, AFM, and LM for surface and internal features, and X-ray scattering methods like SAXS and WAXS for nanoscale organisation [8]. Understanding the morphology of a hydrogel allows us to understand the hydrogels other characteristics like swelling, and mechanical strength better.

4.3.5 Thermal Robustness

Thermal robustness describe how hydrogels respond to temperature changes, including thermal stability, glass transition temperature (T_g), initial decomposition temperature (IDT), and degree of crystallinity. It is measured using thermogravimetric analysis (TGA) for weight changes and differential scanning calorimetry (DSC) for heat flow and thermal transitions [8, 44]. Understanding the thermal properties of a hydrogel allows us to determine the hydrogel's stability and performance in environments with temperature fluctuations.

4.3.6 Texture

Texture describes the physical feel and consistency of hydrogels, including properties such as firmness, cohesiveness, adhesiveness, and viscosity. It is measured using texture analysers that perform compression and extension tests to quantify properties like firmness and consistency [8]. Understanding the texture allows us to better understand the user experience and applicability of the hydrogels.

4.3.7 Biocompatibility

Biocompatibility describes how well hydrogels interact with biological systems without causing harmful effects. It is measured through in vitro and in vivo testing to assess cytotoxicity, such as using MTT assays to determine cell viability [8, 3]. Understanding the biocompatibility of a hydrogel allows us to ensure the hydrogel can be safely used in medical, pharmaceutical, and tissue engineering applications.

4.4 Classification of Conductive Hydrogels

Conductive hydrogels are a specialised subclass of hydrogels designed to merge the soft and flexible nature of traditional hydrogels with the electrical properties of conductive components. On a molecular level conductive hydrogels are a three-dimensional network of polymers infused with conductive elements such as ionic species, conductive polymers (e.g., PEDOT:PSS, polypyrrole), carbon-based nanomaterials (e.g., carbon nanotubes, graphene), or metal nanoparticles. Their conductivity arises through two primary mechanisms: ionic conduction (via mobile ions in the hydrogel matrix) and electronic conduction (through percolation pathways formed by conductive additives) [39].

Previous papers do not provide a universally standardised classification system for conductive hydrogels; however, there is broad consensus on two primary frameworks. Conductive hydrogels can be classified as *electronic conductive hydrogels* (E-CHs) when incorporating filler-type (e.g., carbon nanotubes, MXenes) or conductive polymer-type components, or *ionic conductive hydrogels* (I-CHs) when relying on ionic species (e.g., LiCl, polyelectrolytes). Conductive Hydrogels can also be categorised by the structure of their polymer network, including *single-* (SN), *double-* (DN), or *triple-network* (TN)

4.4. CLASSIFICATION OF CONDUCTIVE HYDROGELS

structures [39, 44]. See Figure 4.2 for a visual summary outlining these two classification frameworks, informed by [39, 44].

Classification By Conductive Material

- **Filler-Type:** Filler-type E-CHs (sometimes referred to as nanomaterial hydrogels) incorporate conductive nanomaterials like carbon nanotubes (CNTs), MXene, or metal nanowires, which form percolation networks for electron transport, achieving high conductivity and strain sensitivity but are inherently toxic, and often sacrifice transparency and mechanical stretchability due to filler aggregation [39].
- **Conductive Polymer-Type:** Conductive polymer-type E-CHs (sometimes referred to as electrical hydrogels) utilise intrinsically conductive polymers e.g., PEDOT:PSS, polyaniline polymerised within the hydrogel matrix, leveraging conjugated π -bond systems for electron flow; these offer uniform dispersion and stretchability but may exhibit opacity and reduced biocompatibility [39].
- **Ionic-Type:** Ionic-type I-CHs rely on mobile ions (e.g., Na^+ , Fe^{3+}) dissolved in an aqueous phase to enable conductivity via ion migration. They are typically simple to fabricate, highly stretchable, transparent, environmentally resilient, and exhibit favourable biocompatibility. However, they face challenges such as conductivity loss due to dehydration [39].

Filler-type E-CHs offer high conductivity and sensitivity for advanced sensors but often lack transparency and stretchability. Conductive polymer-type E-CHs balance conductivity and flexibility, suiting wearable electronics. I-CHs are ideal for transparent, resilient applications like optoelectronics, but can suffer from dehydration and lower conductivity.

Classification By Polymer Network Structure

- **Single-Network:** SN hydrogels consist of a single polymer matrix (e.g., PVA) with embedded conductive components. They are simple to fabricate but often trade mechanical robustness for flexibility, e.g., PVA/AgNWs [39].
- **Double-Network:** DN hydrogels integrate two interpenetrating polymers (e.g., PVA/sodium alginate), combining rigid and flexible networks to enhance toughness and stretchability. For instance, PVA/PAA/ Fe^{3+} DN hydrogels [39].
- **Triple-Network:** TN hydrogels add a third network (e.g., dynamic bonds for self-healing), enabling multifunctionality but increasing synthesis complexity. TN systems often incorporate components like zwitterionic monomers for anti-freezing, or moisture retention [39].

Single Network hydrogels suit simple applications, Double Network structures balance conductivity and durability, and Triple Network designs target advanced functionalities like environmental adaptability.

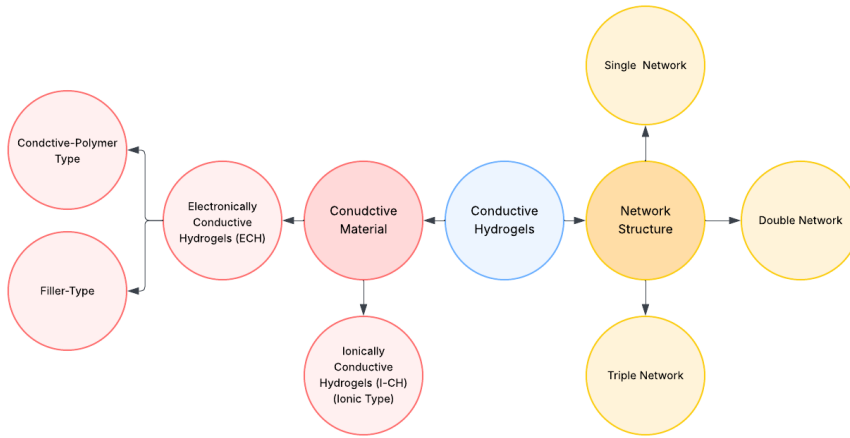


Figure 4.2: A visual summary of the two key conductive hydrogel classification frameworks. The central node represents conductive hydrogels as a material subclass, branching into two major frameworks: **Conductive Material Type**, which distinguishes between electronically conductive hydrogels (E-CHs)—including filler-type and conductive-polymer type—and ionically conductive hydrogels (I-CHs); and **Network Structure**, which categorises hydrogels based on their polymer architecture into single, double, or triple networks. Informed by [39, 44].

4.5 Characteristics of Conductive Hydrogels

Conductive hydrogels retain the core characteristics of traditional hydrogels (e.g., swelling, mechanical properties, morphology) but introduce additional characteristics tied to their electrical functionality and application-specific performance [44].

Electrical Conductivity

Electrical conductivity describes the hydrogel's ability to transport electrical charge via electrons or, more commonly in hydrogels, via mobile ions. Electrical resistance (R) can be measured using complex impedance spectroscopy on an electrochemical workstation, and the conductivity (σ) calculated using the relation:

$$\sigma = \frac{L}{AR}$$

where L is the distance between electrodes, A is the cross-sectional area of the hydrogel sample, and R is the measured resistance. The resulting conductivity values, are reported in Siemens per meter (S/m) [44]. Understanding the conductivity of a hydrogel allows us to design a hydrogel with sufficient conductivity for its intended application.

Sensitivity

Sensitivity quantifies how the hydrogel's electrical resistance changes in response to mechanical deformation. It is measured by calculating the gauge factor (GF), defined as the ratio of relative resistance change to applied strain [44]. Understanding the sensitivity of a hydrogel allows us to determine if it is suitable for its intended application.

Hysteresis

Hysteresis in hydrogel-based sensors describes the delayed electrical response to mechanical strain, which manifests as a residual resistance changes even after strain removal . This residual resistance arises from energy dissipation during cyclic deformation and is quantified by the percentage difference between areas under loading (strain application) and unloading (strain release) curves in resistance-strain plots:

$$\text{Hysteresis (\%)} = \frac{\text{Area between curves}}{\text{Total area under loading curve}} \times 100$$

[44]. Understanding hysteresis in hydrogel-based sensors is essential for applications involving dynamic and cyclic strain, such as skin-mounted wearable, where precise, real-time signal recovery during repetitive motions (e.g., joint movement) ensures sensor accuracy and longevity.

Transparency

Transparency refers to the hydrogel's optical clarity. It is measured using real-time Fourier transform infrared spectrometer [44]. Understanding the transparency of a hydrogel allows us to understand the hydrogels suitable for its indented use, for example a electronic skin or optical sensors require visual feedback and thus high transparency.

Note on Ionogels

Note that Ionogels are three-dimensional polymer networks categorised by their dispersion medium: hydrogels (water-based), organogels (organic solvent-based), and ionogels (ionic liquid-based) [8]. Ionogels replace water or organic solvents with ionic liquids (ILs)—room-temperature, liquid salts composed of bulky organic cations and anions. These ILs enable the gel to be non-volatile, have exceptional thermal stability, and intrinsic ionic conductivity, they can be electrochemically stable at voltages far exceeding hydrogels, and eliminate the risk of dehydration [44].

4.6 Developing an Enriched Composite Hydrogel For Wearable Displays

We developed a PAA/GE [BMIM]TfO composite hydrogel using gelatin (GE), and polymerising acrylic acid (AA) in a water/ionic liquid (IL) mixture:[BMIM]TfO. The obtained hydrogel exhibited high transparency, excellent stretchability, strong self-adhesion, high electrical conductivity, and implicit biocompatibility, making it well suited for applications in wearable electronic displays. This hydrogel is intended to replace the e-ink adhesive layer of a traditional e-ink display stack with a flexible, non-toxic material.

4.6.1 Classification and Characterisation

Based on our outlined classification system, the final PAA/GE [BMIM]TfO composite hydrogel can be provisionally classified across four standard hydrogel classification categories: source: **hybrid**, crosslinking method: **chemically crosslinked**, charge: **anionic**, and conductive material: **ionically conductive (I-CH)**.

In terms of characterisation, the hydrogel exhibited **high transparency**, **strong self-adhesion**, **excellent mechanical robustness**, **high conductivity**, and **implicit biocompatibility**.

Hydrogel Classification

- **Source:** The hydrogel is a **hybrid** material, incorporating a combination of synthetic and natural sources, synthetic monomer (acrylic acid) and a natural biopolymer (gelatin). [8].
- **Preparation Method:** The formulation incorporates both poly(acrylic acid) (PAA) and gelatin, which suggests a copolymeric structure. However, without direct analytical evidence (e.g., FTIR, NMR, or XPS) to confirm covalent integration or molecular-scale interaction between the two polymers, it remains unclear whether true copolymerisation occurs or if gelatin remains physically blended. As such, this classification remains **unknown** without access to suitable imaging and analytical equipment. The term **composite hydrogel** is more appropriate until further characterisation is possible [8].
- **Crosslinking Method:** The hydrogel is **chemically crosslinked**, as polymerisation occurs via free-radical photopolymerisation of AA using PEGDA as a crosslinker and LAP as a photoinitiator, that forms a covalently bonded polymer network [8, 44].
- **Charge of Polymeric Chain:** The resulting hydrogel is **anionic**, due to the dissociation of carboxylic acid groups ($-COOH$) along the PAA backbone (carboxylic acid groups ($-COOH$) are regularly attached to each repeating unit of the poly(acrylic acid) chain) in aqueous and ionic liquid media, imparting a net negative charge [39, 8].

Conductive Hydrogel Classification

- **Conductive Material:** The hydrogel is classified as an **ionic conductive hydrogel (I-CH)**, as electrical conduction occurs via **mobile ionic species** (charged particles such as H^+ , OH^-), and the dissociated ions from $[BMIM]TfO$, ($[BMIM]^+$ and $[TfO]^-$) dispersed throughout both the D.M. water and IL. The D.M. water provides a hydrated, high-permittivity (high ability to reduce electrostatic attraction between ions, allowing them to move more freely) medium that supports ion mobility, while the $[BMIM]TfO$ contributes a high concentration of free ions that enhances the overall conductivity. Under an applied electric field, these ions migrate through the polymer matrix, enabling charge transport via ionic conduction (electrical current carried by the movement of charged ions, not electrons), as opposed to the electronic conduction pathways seen in nanofiller, or conductive polymer-based systems [39, 44, 8].
- **Network Structure:** While the PAA forms the covalently crosslinked network, and gelatin is incorporated as a non-crosslinked additive, without structural characterisation (e.g., SEM or SAXS), there is no direct evidence to determine whether gelatin chains interpenetrate the PAA matrix or remain physically separate, therefore the structure may be a single-network hydrogel or a semi-interpenetrating polymer network (semi-IPN). This classification remains **unknown**, without access to suitable imaging and analytical equipment [8].

Note on Medium Composition

Although enriched with the ionic liquid $[BMIM]TfO$, the hydrogel does not meet the criteria of an ionogel, as its dominant dispersion medium remains D.M. Water. It is best described as an **ionically enriched hydrogel**, combining the water-based benefits of hydrogels with enhanced conductivity and stability from the IL [44, 8].

4.6.2 Functional Characteristics

The required characteristics of a hydrogel for use in a wearable display were high transparency, mechanical robustness, strong self adhesion, high conductivity, and implicit biocompatibility. Based on these requirements, the final hydrogel was evaluated across four key characteristics using a combination of available quantitative measurements and qualitative assessments. However due to equipment limitations, only electrical conductivity was quantified; other properties were assessed via observational methods. Comprehensive characterisation was not possible within the scope of this work as it would require access to specialised equipment.

- **Electrical Conductivity:** Quantified using a benchtop conductivity meter and multimeter. The gel exhibited **high ionic conductivity (22 mS)** and **low electrical resistance (~0.05 MΩ)**.
- **Transparency:** Assessed qualitatively via visual inspection by simply placing samples over sticky notes with written text. Optical clarity appeared high. Quantitative measurement would require a Fourier transform infrared spectrometer.
- **Self-Adhesion:** Evaluated manually through repeated peeling and reapplication. The hydrogel displayed strong adherence to gloved hands and smooth surfaces. Quantitative analysis would require a texture analyser for measuring adhesive force.
- **Mechanical Robustness:** Determined through manual deformation and handling. The gel demonstrated good flexibility and integrity under light bending and compression. Accurate mechanical characterisation (e.g., tensile strength, modulus) would require equipment such as a Dynamic Mechanical Analyser (DMA).
- **Biocompatibility:** While the hydrogel can be said to be **implicitly biocompatible** as all constituent materials (PAA, gelatin, $[BIMM]TfO$, PEGDA, LAP, water) are individually known to be biocompatible, used in biomedical contexts, or constituent materials in hydrogels used in on-skin applications [35, 44], the biocompatibility of the resulting hydrogel formulation has not been experimentally confirmed. Formal biocompatibility testing (e.g., cytotoxicity or sensitisation assays) would be required to verify its safety for direct skin contact or long-term use.

PAA/GE [BMIM]TfO Hydrogel Synthesis Protocol (Final Recipe)

This step-by-step protocol details the procedure for synthesising the D.M Water/[BMIM]TfO-based PAA/GE composite hydrogel, which was ultimately identified as the most optimal formulation out of the candidate hydrogels we synthesised for a wearable E-Ink display.

Required Equipment:

- Magnetic stirrer with adjustable temperature and speed
- 405 nm UV curing light
- Laboratory scales (precision to at least 0.01 g)
- Mixing beaker (e.g., 50 mL)
- Pipettes (with appropriate volumes)
- Micro-spatula

Ingredients (All from Sigma-Aldrich):

- Deionised Water (D.M Water)
- Acrylic Acid (AA)
- Gelatin Type B (GE)
- 1-butyl-3-methylimidazolium trifluoromethanesulfonate ([BMIM]TfO)
- Poly(ethylene glycol) diacrylate (PEGDA)
- Lithium phenyl-2,4,6-trimethylbenzoylphosphinate (LAP)

Step-by-Step Instructions:

1. Place the empty mixing beaker on the balance and **tare** (zero) it.
2. Using a pipette, add **5.6 g of deionised water (D.M Water)**. Tare the scale again.
3. Add **5.1 g of [BMIM]TfO** via pipette. Tare again.
4. Add **1.8 g of acrylic acid (AA)** via pipette. Tare again.
5. Add **0.5 g of PEGDA** via pipette. Tare again.
6. Add **0.45 g of gelatin (GE)** using a micro-spatula. Tare again.
7. Add **0.05 g of LAP** using a micro-spatula. If the balance is not sensitive enough, estimate a small quantity using a micro-spatula.
8. Place a magnetic stir bar in the beaker and transfer the beaker to the magnetic stirrer apparatus.
9. Set the stirrer temperature to **50°C** and the stir speed to **level 5**. Stir for **10 minutes**.
10. After 10 minutes, stop the stirrer. Visually confirm that the solution is homogenous; if not, continue stirring until fully mixed.
11. Pour the prepared solution into a mold of desired shape.
12. Place the **405 nm UV light** directly above the mold and expose it for **3 minutes**.
13. Switch off the UV light. The hydrogel is now cured and can be carefully removed from the mold for testing.

4.6.3 Clarification of Naming Conventions

Gels are typically named by listing the main polymers (using standard abbreviations, e.g., PVA) in order of proportion or significance. When additional components (like nanoparticles or fillers) are added, “composite” can be included in the name (e.g., “PVA/AgNPs composite hydrogel”). If a functional ionic liquid is present, its abbreviation is included (e.g., “[BMIM]TfO-enriched hydrogel”) to highlight its role. The gel type: hydrogel, ionogel, or organogel, is specified based on the liquid phase (e.g., a hydrogel contains mostly water as the continuous liquid phase). If multiple solvents, gel types, or polymer sources are combined, “hybrid” is added to indicate multifunctionality.

4.6.4 Experimental protocol

In order to replace the E-Ink adhesive layer in an E-Ink display stack, our hydrogel had to have high transparency, excellent stretchability, strong self-adhesion, high conductivity, and implicit biocompatibility, and given the constraints in equipment and time, the fabrication process had to be rapid, and simple.

Note the materials list and their respective supplier for the experiments conducted in this study are as follows: Acrylic acid (AA), gelatin (Type B), polyvinyl alcohol (PVA), polyvinylpyrrolidone (PVP), deionised water (D.M water), 1-butyl-3-methylimidazolium trifluoromethanesulfonate ([BMIM]TfO), poly(ethylene glycol) diacrylate (PEGDA), and lithium phenyl-2,4,6-trimethylbenzoylphosphinate (LAP) were all procured from Sigma-Aldrich.

Method

To meet the demands of the experiment, we focused on a facile one-pot photopolymerisation approach, leveraging poly(ethylene glycol) diacrylate (PEGDA) as the crosslinker, lithium phenyl-2,4,6-trimethylbenzoylphosphinate (LAP) as the photo-initiator, and only biocompatible materials.

Multiple gel formulations were prepared via one-pot photopolymerisation, using D.M. water as the solvent, [BMIM]TfO as the ionic liquid, AA as a monomer, PVA and GE as polymers, GE and PVP as functional additives, LAP as the photo-initiator, and PEGDA as the crosslinker. Briefly, varying amounts of D.M. water, [BMIM]TfO, AA, PVA, GE, PVP, LAP, and PEGDA were mixed. PEGDA (0.5 g), and LAP (0.05 g) were used in all formulations unless otherwise specified. The mixture was mixed on a magnetic stirrer until a homogeneous solution was obtained. Then, the solution was transferred into a mold, and irradiated under 405 nm UV light (intensity: 30 mW/cm²) until gelation.

To evaluate the suitability of various hydrogel formulations, a series of candidate gels were synthesised using a one-pot photopolymerisation approach. We began by testing polymer-based hydrogels incorporating different structural additives (e.g., PVA, GE, PVP) in water (see Table 4.1). We then explored acrylic acid (AA)-based formulations combined with the ionic liquid [BMIM]TfO, testing different concentrations and additives such as gelatin and PVP (see Table 4.2). To ensure consistent polymerisation and reproducibility across samples, each gel was processed under controlled stirring and UV curing conditions. See Table 4.3 for the specific temperature, stirring intensity, duration, and UV exposure time used for each formulation.

Model	Water (g)	PAA (g)	PVA (g)	GE (g)	PVP (g)
Control	10.9	—	—	—	—
PVA	10.9	—	1.8	—	—
PVA/PVP	10.9	—	1.8	—	0.3
GE	10.9	—	—	0.45	—
GE/PVP	10.9	—	—	0.45	0.3

Table 4.1: Formulations of polymer-based hydrogels using D.M. Water as the primary solvent, with variations in the inclusion of PVA, GE, and PVP as structural and functional additives. PEGDA (0.5 g) and LAP (0.05 g) were used in all formulations.

Model	Water (g)	[BMIM]TfO (g)	AA (g)	GE (g)	PVP (g)
[BMIM]TfO AA	2.75	2.75	0.9	—	—
D.M Water/[BMIM]TfO PAA	2.75	2.75	0.9	—	—
D.M Water/[BMIM]TfO PAA/PVP	2.75	2.75	0.9	—	0.3
D.M Water/[BMIM]TfO PAA*	5.6	5.1	1.8	—	—
D.M Water/[BMIM]TfO PAA/GE	5.6	5.1	1.8	0.45	—

Table 4.2: Formulations of acrylic acid (AA)-based hydrogels incorporating the ionic liquid [BMIM]TfO, with optional inclusion of gelatin (GE) and PVP. D.M Water was used as a co-solvent. PEGDA (0.5 g) and LAP (0.05 g) were used in all formulations.

Model	Stir Temp (°C)	Stir Strength	Stir Time (s)	UV Time (s)
Control	40	3	600	600
PVA	90	5	3600	600
PVA/PVP	50	5	600	600
GE	50	3	600	600
GE/PVP	50	3	3600	600
[BMIM]TfO AA	50	5	600	180
D.M Water/[BMIM]TfO PAA	50	5	600	180
D.M Water/[BMIM]TfO PAA/PVP	50	5	3600	180
D.M Water/[BMIM]TfO PAA*	50	5	600	180
D.M Water/[BMIM]TfO PAA/GE	50	5	600	180

Table 4.3: Magnetic stirring and UV curing conditions used for each hydrogel formulation. Conditions were adjusted to ensure homogenisation and consistent crosslinking across different compositions.

4.6.5 Characterisation

To evaluate the practical performance of each hydrogel formulation, both quantitative and qualitative metrics were assessed. Electrical conductivity and resistance were measured using a benchtop conductivity meter, and a digital multimeter, respectively. Due to the absence of specialised testing equipment, properties such as transparency, mechanical robustness, and self-adhesion were assessed qualitatively through visual inspection and manual manipulation.

See Table 4.4 for a side-by-side comparison of the key performance characteristics relevant to the hydrogel’s intended use in a wearable E-Ink display, highlighting the trade-offs between the necessary electrical and physical properties across candidate gels. Conductivity is reported in mS where applicable, resistance is shown in MΩ, and visual traits are noted as binary yes/no outcomes based on observational criteria. See also Figure 4.3 for photographs of a selection of synthesised hydrogels, offering a visual sense of their form, and optical clarity.

Model	Conductivity	Resistance	Transparent	Mechanically Robust	Self-Adhesive	Conductive
Control	—	15 MΩ	Yes	No	No	No
PVA	—	12.0 MΩ	No	No	No	No
PVA/PVP	—	11 MΩ	No	No	No	No
GE	—	1 MΩ	Yes	No	Yes	Yes
GE/PVP	—	0.9 MΩ	No	No	Yes	Yes
[BMIM]TfO PAA Model	—	0.3 MΩ	No	No	No	Yes
D.M Water/[BMIM]TfO PAA	—	0.4 MΩ	Yes	No	No	Yes
D.M Water/[BMIM]TfO PAA/PVP	25 mS	0.1 MΩ	No	No	No	Yes
D.M Water/[BMIM]TfO PAA*	26 mS	0.1 MΩ	Yes	Yes	Yes	No
D.M Water/[BMIM]TfO PAA/GE	22 mS	0.05 MΩ	Yes	Yes	Yes	Yes

Table 4.4: Hydrogel model characteristics with both measured electrical performance, and qualitatively assessed physical properties. Conductivity (mS) and resistance (MΩ) were measured using standard instrumentation, while transparency, mechanical robustness, and self-adhesion were evaluated through visual inspection and manual testing. “Yes”/“No” entries reflect whether each model qualitatively met our predefined criteria for those properties. The final “Conductive” column indicates whether the material demonstrated adequate conductivity for potential use in a wearable E-Ink display, with a “Yes” assigned to samples exhibiting a resistance of 1 MΩ or less.

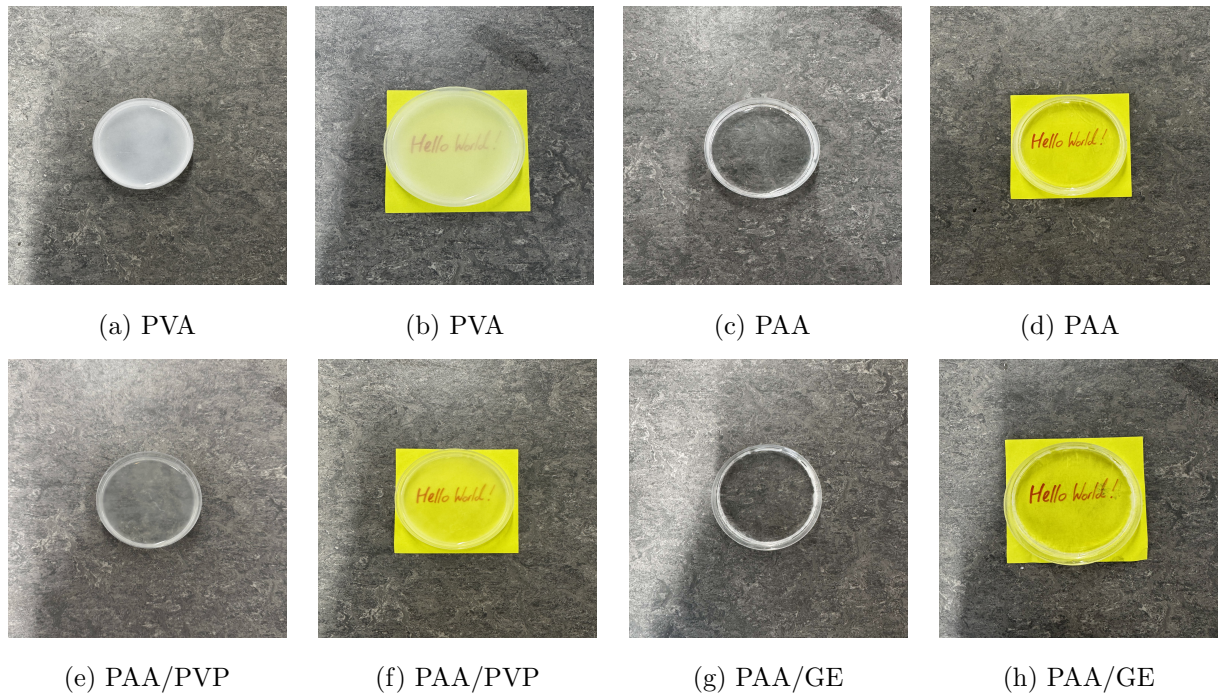


Figure 4.3: Photographs of a selection of synthesised hydrogel formulations. Images correspond to selected candidate gels from Tables 4.1, 4.2, 4.3, and 4.4. Each pair of images shows: (1) the hydrogel sample in isolation, and (2) the same sample placed on top of a sticky note with written text for a sense of the hydrogel's optical clarity. Shown are: (a) PVA, (b) PVA on sticky note, (c) [BMIM]TfO PAA Model, (d) [BMIM]TfO PAA Model on sticky note, (e) D.M Water/[BMIM]TfO PAA/PVP, (f) D.M Water/[BMIM]TfO PAA/PVP on sticky note, (g) D.M Water/[BMIM]TfO PAA/GE, (h) D.M Water/[BMIM]TfO PAA/GE on sticky note. Samples visibly differ in form, and optical clarity, reflecting their underlying material compositions, and stirring and UV curing conditions.

4.7 Results and Discussion

Among all the formulations tested, the hydrogel that demonstrated the best overall performance was the D.M Water/[BMIM]TfO PAA/GE composite. This formulation exhibited the highest conductivity (22 mS), lowest resistance ($0.05\text{ M}\Omega$), excellent transparency, strong self-adhesion, and high mechanical robustness (Table 4.4). These characteristics made it the most suitable candidate for replacing the adhesive layer in our wearable E-Ink display stack.

This hydrogel was developed by modifying the ionogel architecture introduced by Yuan et al. [44], which originally used Irgacure 1173 as a photoinitiator in a purely ionic liquid matrix. While promising in terms of conductivity and stretchability, the Yuan et al. system potentially lacked implicit biocompatibility due to the use of Irgacure 1173.

To address this, we replaced Irgacure with lithium phenyl-2,4,6-trimethylbenzoylphosphinate (LAP), a biocompatible, water-soluble photoinitiator. This substitution necessitated the addition of water to the formulation. However, the introduction of water decreased the mechanical stability of the gel, which we countered by incorporating gelatin (GE) as a structural additive. The resulting D.M Water/[BMIM]TfO PAA/GE composite hydrogel retained the core benefits of the Yuan et al. system while achieving improved implicit biocompatibility and mechanical performance suited for on-skin electrophoretic display applications.

Thus after systematic formulation screening and optimisation, we successfully fabricated a highly transparent, mechanically robust, self-adhesive, and conductive hydrogel through facile one-pot, photopolymerising AA in a Water/IL mix:[BMIM]TfO with the addition of a functional additive GE and a crosslinker PEGDA.

In contrast to conventional adhesive layers in E-Ink displays, this hydrogel is flexible while remaining transparent, adhesive, and conductive, without requiring toxic materials or complex synthesis, demonstrating that a hydrogel can meet the functional requirements for use in a novel wearable electrophoretic display stack, and provide a promising foundational material for use in a wearable electronic display.

However, although the hydrogel can be said to be implicitly biocompatible, verifying the hydrogel's biocompatibility and functional properties remains a significant challenge, necessitating rigorous laboratory-based characterisation and standardised biocompatibility testing before it can be safely integrated beyond a prototype e-ink display or applied directly to the skin.

Chapter 5

Part 3: Display Integration

In this chapter, we begin by introducing the fundamental mechanisms underlying traditional E-Ink displays, with particular emphasis on the principles of image formation and control. This includes key processes such as electrophoretic motion, grayscale rendering, and waveform design, which together determine how content is displayed and updated. Emphasis is placed on these mechanisms because an understanding of display physics, including limitations such as grayscale degradation, DC imbalance, and ghosting is essential if a high resolution wearable E-Ink display is to be realised. Such a display will eventually require optimised driving waveforms, lookup tables, and control schemes that reliably reproduce and refresh content.

We then examine the layered architecture and material composition typically used in these systems. Emphasis is placed on understanding the display stack architecture as this forms the critical foundation for any attempt to modify or re-engineer a traditional E-Ink display for wearable use. Building on this foundation, we then present our approach to developing a novel display stack tailored for wearable E-Ink applications.

5.1 Introduction to E-Ink Displays

E-Ink displays are a type of electrophoretic display (EPD) [15], that generate images by precisely controlling the distribution of charged pigment particles suspended within a non-polar dielectric fluid inside of millions of microscopic capsules, each approximately 40 microns in diameter [42]. These capsules contain a clear dielectric fluid with suspended pigment particles: positively charged black particles (carbon black) and negatively charged white particles (titanium dioxide). When an electric field is applied, the particles migrate within the fluid, altering the visible colour of the display [11].

When a positive voltage is applied to the pixel electrode, an electric field is established that drives positively charged black particles downward toward the common electrode and negatively charged white particles upward toward the viewing surface, producing a white visual state. Conversely, applying a negative voltage reverses the electric field, driving black particles upward and white particles downward, resulting in a black appearance [14].

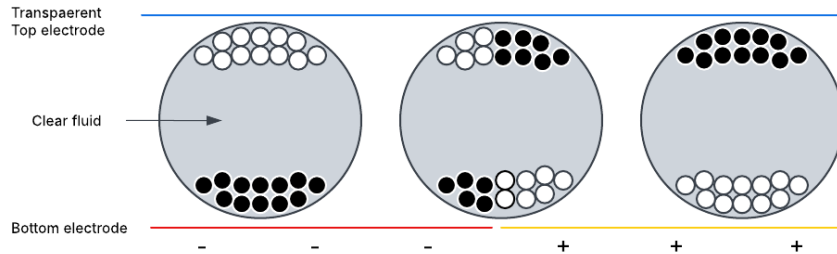


Figure 5.1: Cross-sectional diagram of an E-Ink microcapsule. An electric field applied between the top and bottom electrodes causes charged black and white pigment particles to migrate within the capsule, controlling the pixel's visible state. This electrophoretic mechanism enables bistable and reflective display behaviour.

5.2 Image Formation and Control in E-Ink Displays

Unlike traditional displays where a pixel's colour can be directly set (e.g., “set pixel to the RGB of black”) electrophoretic displays rely on the controlled distribution of charged pigment particles suspended in a dielectric fluid to display colour. Achieving a colour in an electrophoretic display requires not a single command, but a precisely timed sequence of voltage pulses. This sequence, known as a **driving waveform**, defines not just the amplitude, but also the polarity and duration of each voltage pulse applied to the electrodes over time in order to distribute the particles and produce a target colour at each pixel [14]. In an E-Ink displays, these waveforms are delivered to pixel electrodes controlled by a matrix of thin-film transistors (TFTs), using coordinated row-column addressing. The TFTs act as switches, enabling each pixel electrode to receive a unique waveform during its addressed row period [5].

In a typical waveform sequence, the particles are first activated by alternating “shaking” pulses, which mobilise them within the fluid allowing them to overcome particle adhesion and aggregation within the capsule, and ensuring that the particles can respond uniformly to subsequent driving pulses. Next, the particles are driven toward the top and bottom boundaries of the capsule to remove any image history, followed by a targeted voltage sequence that positions the particles into a specific arrangement corresponding to the intended gray level [40]. See Figure 5.2 for the track of a particle in a pixel with top and bottom electrodes during a waveform cycle.

However, as the particles are driven to specific states (graylevels), residual effects can occur due to the dependence of the final reflectivity on previous particle distributions. This can result in discrepancies between the target grayscale and the actual grayscale. This effect leads to a phenomenon known as **ghosting**, where the current image appears partially superimposed with traces of the prior one [40, 14]. See 5.2, where (GT) represents the intended grayscale target, and (GT*) the actual reflectivity achieved.

While electrophoretic displays are designed to be bistable, meaning the particle distribution, and thus the displayed image, remains unchanged after the removing the driving voltage, in reality the particle distribution is usually influenced by the built-in electric field (a persistent internal field caused by trapped charges, ionic impurities, or material asymmetries, which exists even when no external voltage is applied) of each charged species (charged molecules or atoms present in the display) which can gradually disturb the particle distribution. This slow drift in particle distribution leads to a subtle but progressive change in reflectivity, resulting in a degradation of the intended grayscale. This phenomena is referred to as **grayscale degeneration** [40]. See Figure 5.2 where (GT*) is the achieved grayscale value and (GD*) the degenerated grayscale value over time.

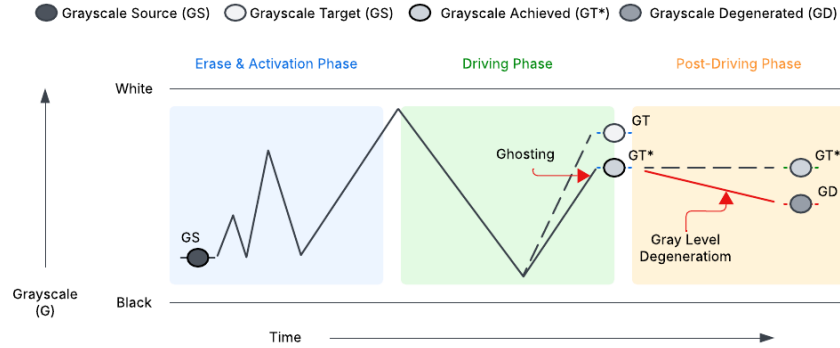


Figure 5.2: Schematic optical trace showing particle movement and reflectivity changes in an electrophoretic display (EPD) during the driving waveform, showing time-based progression from the intended grayscale target (GT), to the achieved reflectivity (GT*), and the subsequent decline due to grayscale degeneration (GD*).

Additionally, grayscale degradation can occur in areas of static display, i.e. when the same image stays on the screen for a long time. In these areas the particles are repeatedly driven in the same direction over a long period of time, which leads to the gradual build up of charge in the direction the display's built-in electric field. The resulting charge accumulation is referred to as **DC imbalance**. The driving waveform is designed to control pigment particle movement while minimising visual artifacts caused by the phenomena of ghosting, grayscale degradation, and DC imbalance [40].

A typical driving waveform consists of a three-phase sequence: Erase, Activate, and Display. The Erase phase begins with a high-voltage reset pulse (often preceded by a short help-reset pulse of opposite polarity) that drives all pigment particles to a uniform optical extreme, either full white or full black, effectively clearing any residual image and reducing ghosting. This phase may include brief shaking pulses, and alternating voltages, to pre-activate particles and re-energise them. Following erasure, the activation phase again restores particle mobility and establishes a consistent baseline grayscale across all pixels. This is typically achieved through additional shaking pulses. Finally, the Display phase applies targeted driving pulses to position pigment particles according to the desired grayscale level for each pixel, which renders the new image [40, 14]. See Figure 5.3 for the structure of a typical waveform.

To render multi-level grayscale during this Display phase, EPDs commonly employ two modulation techniques: Pulse Amplitude Modulation (PAM) and Pulse Width Modulation (PWM). In PAM, the grayscale level is adjusted by varying the amplitude of the voltage pulse while keeping its duration constant. Higher voltage amplitudes generate stronger electric fields, leading to greater pigment particle displacement and consequently lighter or darker pixel reflectance, depending on the polarity of the applied voltage. Conversely, PWM achieves grayscale control by varying the duration of the voltage pulse while maintaining a fixed amplitude, longer pulses allow more particles to migrate, resulting in more pronounced changes in visual appearance. Both modulation strategies influence the final particle distribution of the pigment particles within each microcapsule, and this distribution directly determines the pixel's optical reflectance and perceived grayscale level [40]. See Figure 5.4 for the structure of PAM and PWM driving pulses.

To mitigate against DC Imbalance and prevent long-term damage and maintain display quality, waveforms are also carefully designed to ensure DC Balance (the net integral of voltage over time at each pixel is approximately zero). This is achieved through a combination of local DC balance (within each pixel's waveform cycle) and global DC balance (across the full display) [40].

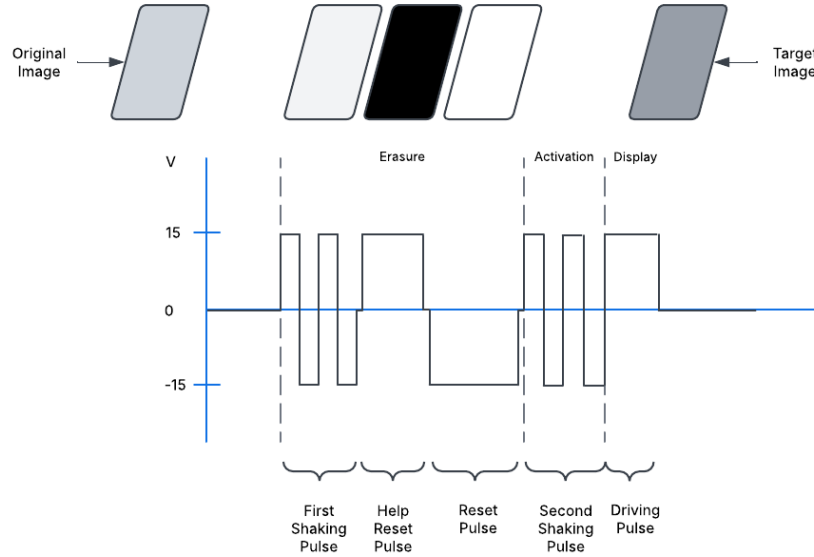


Figure 5.3: The general structure of a modified waveform for EPD (electrophoretic display) driving, showing the typical three-phase sequence: Erase (reset and shaking), Activate (particle mobilisation), and Display (grayscale rendering). This structure is designed to minimise visual artifacts such as ghosting, grayscale degradation, and DC imbalance.

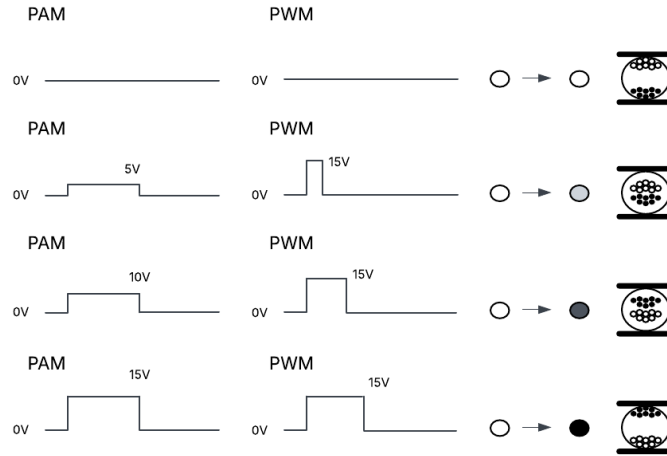


Figure 5.4: Driving pulses for a multi-grayscale electrophoretic display using Pulse Amplitude Modulation (PAM) and Pulse Width Modulation (PWM). PAM varies voltage amplitude, while PWM varies pulse duration to control pigment particle displacement.

Electrophoretic displays are highly sensitive; small changes in particle size, material composition, or zeta potential (the electrical charge on the surface of the particles that affects how easily they move in a liquid) can significantly impact performance. Even within the same batch, prior voltage histories can alter particle behaviour, making consistent grayscale rendering difficult. To manage this complexity, manufacturers rely on lookup tables (LUTs): predefined datasets that map every possible grayscale transition (from a given starting shade to a target shade) to a specific, empirically optimised driving waveform. These LUTs are built through extensive testing, measuring particle displacement and reflectance under varying conditions [40].

5.3 Layered Architecture and Material Composition of E-Ink Displays

E-Ink displays are composed of a multi-layered structure that integrates conductive, adhesive, and structural materials [11, 20]. See Figure 5.5 for a cross-sectional representation of the E-Ink display's layered architecture.

The protective outermost layer serves to shield the underlying components of the E-Ink display from mechanical damage, moisture, and environmental contaminants. This layer must maintain optical clarity, mechanical stability, and flexibility, while also being chemically and UV resistant and ensuring strong adhesion to the adjacent electrode layer. Industrial implementations often use coated or treated PET films [20].

The transparent electrode layer enables the application of electric fields to control the movement of charged pigments. This layer must be electrically conductive, and optically transparent. Industrial implementations often use indium tin oxide (ITO) [20].

The E-Ink microcapsule layer comprises millions of electrophoretic microcapsules embedded within a polymer matrix, which securely holds in place and evenly distributes the microcapsules. The polymer matrix must exhibit chemical compatibility with the microcapsules, optical clarity, flexibility, and allow for strong adhesion to adjacent layers. Manufacturers often use acrylic polymers, urethane-based polymers, and various copolymers [20].

The backplane layer serves as the electronic control system of the E-Ink display, housing a transistor array, which functions as an addressing system, selectively applying voltage to activate specific regions of the display and control the movement of electrophoretic particles. This layer must provide precise electrical control. Manufacturers often use silicon-based thin-film transistor (TFT) substrates [20].

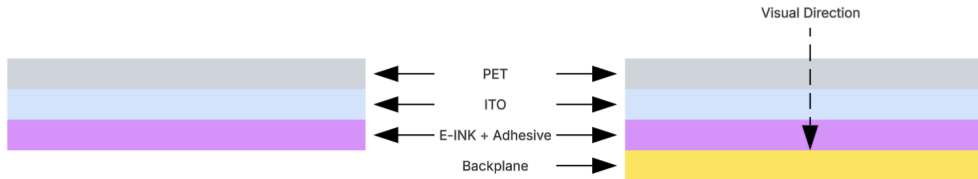


Figure 5.5: Cross-sectional diagram showing the layered architecture of an E-Ink display. The protective outer layer (PET), the transparent conductive layer (ITO), the electrophoretic imaging layer (E-INK + Adhesive) contains pigment-filled microcapsules embedded in a polymer matrix, bonded to the substrate via adhesive's, and the addressing layer (Backplane) contains the circuitry for pixel-level control.

5.4 Developing a Novel Display Stack for Wearable E-Ink Displays

We developed a prototype single-segment E-Ink display incorporating a custom-formulated biocompatible microcapsule dispersion embedded within our synthesised hydrogel matrix. Our design was intended to serve as a flexible, biocompatible alternative to the conventional microcapsule-polymer and adhesive layers used in commercial E-Ink displays. Transparent flexible indium tin oxide (ITO) films were employed in place of the rigid PET substrates and backplanes typically found in commercial systems, with the top electrode designated as the control (pixel-driving) electrode to accommodate the eventual use of human skin as the bottom electrode. See Figure 5.6 for a cross-sectional representation of the BioPixel prototype display's layered architecture with key differences to traditional displays, such as the replacement of the rigid and toxic adhesive layers of traditional E-Ink displays with biocompatible, flexible components

designed for wearable use.

The prototype aimed to determine whether a fully flexible and biocompatible display stack, capable of conforming to curved and wearable surfaces, could support basic electrophoretic functionality as a foundational step towards a high-resolution wearable E-Ink display. However, despite successful fabrication of the display stack, verification of the electronic control system, and verification of our hydrogel's high conductivity, no electrophoretic switching was observed, highlighting key challenges associated with microcapsule stability during the integration of the current generation of biocompatible E-Ink into our hydrogel.

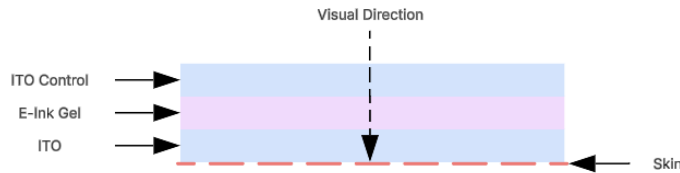


Figure 5.6: Layered architecture of the BioPixel display prototype. Our design replaces the rigid PET and backplane of conventional E-Ink displays with two flexible ITO electrodes, and substitutes the conventional E-Ink microcapsule and adhesive layer with a biocompatible hydrogel-based electrophoretic layer ("E-Ink Gel"). The top ITO layer ("ITO Control") acts as the pixel-driving electrode, while the bottom ITO layer is intended to be removed in future iterations, allowing the wearer's skin, leveraging its natural conductivity, to function as the bottom electrode (contingent on successful biocompatibility validation of the E-Ink Gel).

5.4.1 Microcapsule Stability In PAA/GE/E-Ink Composite Hydrogel

Note the materials used in this study were as follows: Acrylic acid (AA), gelatin (Type B), poly(ethylene glycol) diacrylate (PEGDA), 1-butyl-3-methylimidazolium trifluoromethane-sulfonate ([BMIM]TfO), lithium phenyl-2,4,6-trimethylbenzoylphosphinate (LAP), and deionised water (D.M. Water) were procured from Sigma-Aldrich.

Additionally, four different E-Ink microcapsule aqueous dispersions from 2023 batches were obtained from existing laboratory stock. These included two red-tinted dispersions (Red 1 and Red 2), one white-tinted dispersion (White), and one black-tinted dispersion (Black).

Methods

A. Base Prepolymer Hydrogel Mix

The base prepolymer hydrogel mix was based on the PAA/GE formulation developed in Chapter 4. Specifically, 5.6 g of deionised water, 5.1 g of [BMIM]TfO, 1.8 g of acrylic acid (AA), 0.45 g of gelatin (GE), 0.5 g of poly(ethylene glycol) diacrylate (PEGDA) and 0.05 g of lithium phenyl-2,4,6-trimethylbenzoylphosphinate (LAP) were used in all subsequent experiments.

B. E-Ink Dispersion Selection

Before incorporating E-Ink microcapsules into the hydrogel matrix, each of the four available 2023 stock dispersions, Red 1, Red 2, White, and Black, were evaluated by optical microscopy under consistent optical conditions ($3000\times$ magnification) to assess microcapsule integrity and dispersion uniformity. Among the tested samples, the White dispersion exhibited the highest proportion of intact microcapsules, with minimal aggregation and rupture. Based on these observations, the White E-Ink dispersion was selected for subsequent hydrogel incorporation experiments. See Figure 5.7 for the microscopy slide

of the four E-Ink dispersions evaluated for use in the display prototype, used to compare microcapsule integrity and dispersion uniformity.

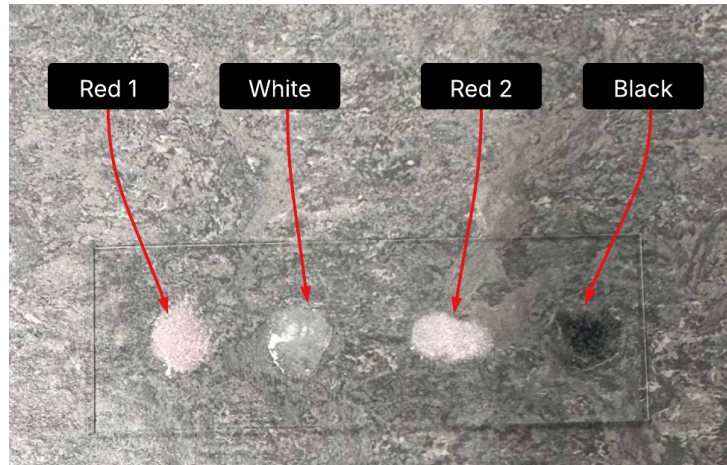


Figure 5.7: Optical microscopy slide of the four evaluated E-Ink dispersions from 2023 laboratory stock, arranged from left to right: Red 1, White, Red 2, and Black.

C. E-Ink Integration Protocols

Following preparation of the base prepolymer mix, four different E-Ink microcapsule integration protocols were evaluated to determine the impact of mixing conditions on microcapsule stability. For all integration tests, a fixed amount of 16 drops of white E-Ink dispersion was incorporated, corresponding to approximately 0.32 g total (at 0.02 g per 0.05 mL drop). See Table 5.1 for the integration protocols tested.

Protocol ID	Before E-Ink Addition	After E-Ink Addition	Timing of E-Ink Addition
Mix-1	50°C, Strength 3, 600 s	—	Before mixing
Mix-2	24°C, Strength 1, 600 s	—	Before mixing
Mix-3	24°C, Strength 1, 600 s	24°C, Strength 1, 300 s	After base mixing
Mix-4	30°C, Strength 3, 600 s	24°C, Strength 1, 300 s	After base mixing

Table 5.1: Four mixing protocols used to incorporate E-Ink microcapsules into the hydrogel matrix. Each protocol varies mixing temperature, intensity, duration, and whether the E-Ink was added before or after base hydrogel mixing.

D. Post-Mixing Microscopy Observations

Microscopy analysis was conducted on the PAA/GE/E-Ink prepolymer mixtures prepared under each mixing protocol to evaluate microcapsule integrity following incorporation.

- **Mix-1:** Severe rupture of microcapsules was observed, with very few intact structures remaining. The stirring strength, and high temperature of 50°C likely contributed to microcapsule damage.
- **Mix-2:** Some intact microcapsules were present, but their distribution throughout the matrix was poor. While lower stirring strength (strength 1) and room temperature helped preserve capsule structure, mixing was insufficient for uniform dispersion.
- **Mix-3:** A moderate number of intact microcapsules were observed, though slight aggregation occurred. Gentle post-addition mixing at room temperature (strength 1) appeared to improve microcapsule survival without significant additional rupture.
- **Mix-4:** Moderate preservation of microcapsules was seen, with relatively even distribution. Initial mixing at 30°C and strength 3 before E-Ink addition, followed by gentle post-addition mixing, provided a balance between dispersion and microcapsule survival.

E. Photopolymerisation Protocols

Based on the post-mixing microscopy observations, Mix-4 was selected as the standard method for E-Ink microcapsule integration.

To evaluate the effect of UV curing on microcapsule integrity, sample mixes were poured into moulds and exposed to 405 nm UV light for different lengths of time. See Table 5.2 for the UV exposure protocols tested.

Protocol ID	UV Exposure Time (s)
Photo-1	30
Photo-2	60
Photo-3	90
Photo-4	120
Photo-5	200

Table 5.2: Photopolymerisation protocols.

F. Post-Photopolymerisation Microscopy Observations

Microscopy analysis was conducted after UV curing to assess the impact of exposure time on microcapsule integrity. See Figure 5.8 for microscopy slides with hydrogel samples cured for different lengths of time.

- **Photo-1:** Minimal additional rupture was observed compared to the prepolymer mix, with most microcapsules remaining intact.
- **Photo-2:** Microcapsule rupture remained low, similar to the 30 s exposure, with good overall preservation of structures.
- **Photo-3:** A slight increase in ruptured microcapsules was noted, but a substantial proportion of intact microcapsules remained.
- **Photo-4:** A rapid decline in intact microcapsules was observed. Significant rupture and loss of structure was evident.
- **Photo-5:** Nearly all microcapsules were ruptured, although the hydrogel mechanical strength was noticeably higher compared to samples cured at shorter exposure times.

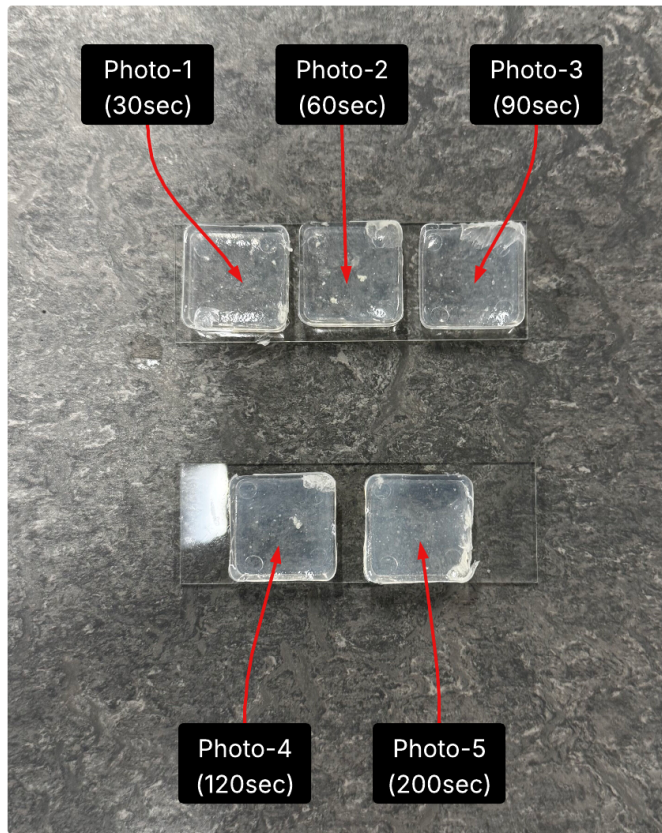


Figure 5.8: Optical microscopy slides of PAA/GE/E-Ink hydrogel samples after Photopolymerisation under different exposure times, arranged from left to right Photo-1 to Photo-5.

5.4.2 Results and Discussion

Based on the initial screening of E-Ink microcapsule dispersions, the White dispersion was selected for integration into the hydrogel matrix due to its superior microcapsule integrity and minimal pre-existing rupture compared to the Red and Black batches.

Among the mixing protocols evaluated, Mix-4 (initial stirring at 30°C and strength 3 prior to E-Ink addition, followed by gentle mixing at 24°C and strength 1) achieved the best balance between microcapsule preservation and dispersion quality. This protocol demonstrated moderate microcapsule survival with relatively uniform distribution within the hydrogel matrix.

Subsequent UV curing trials indicated that Photo-3 (90 s UV exposure at 405 nm) provided the optimal balance between maintaining microcapsule integrity and achieving sufficient mechanical strength of the cured hydrogel. Shorter UV exposures (30 s and 60 s) preserved microcapsules but produced weaker hydrogels, while longer exposures (120 s and 200 s) significantly degraded microcapsule populations despite improving mechanical properties.

Therefore, the combination of White E-Ink dispersion, Mix-4 prepolymer integration protocol, and Photo-3 photopolymerisation protocol was selected as the most promising PAA/GE/E-Ink composite hydrogel candidate for integration into the full display stack.

5.4.3 Electronic Architecture and Control System

Note the materials used in the prototype are as follows: Arduino microcontroller, a dual Single Pole Double Throw (SPDT) relay module, a $\pm 15V$ power supply, and two Indium Tin Oxide (ITO) films. All components were donated by the University of Bristol.

Method

The electronic circuit was assembled utilising the ITO films as the bottom and top conductive electrodes, the Arduino microcontroller as the control signal generator for polarity switching, and the relay module, driven by the Arduino, as the enabler of bidirectional voltage application by alternating the polarity of the voltage supplied to the display. A basic square waveform was implemented by controlling relay timing via Arduino commands, no pulse modulation was used. A square waveform was determined to be sufficient for simple binary black-white switching. See Figure 5.9 for a schematic of the final setup.

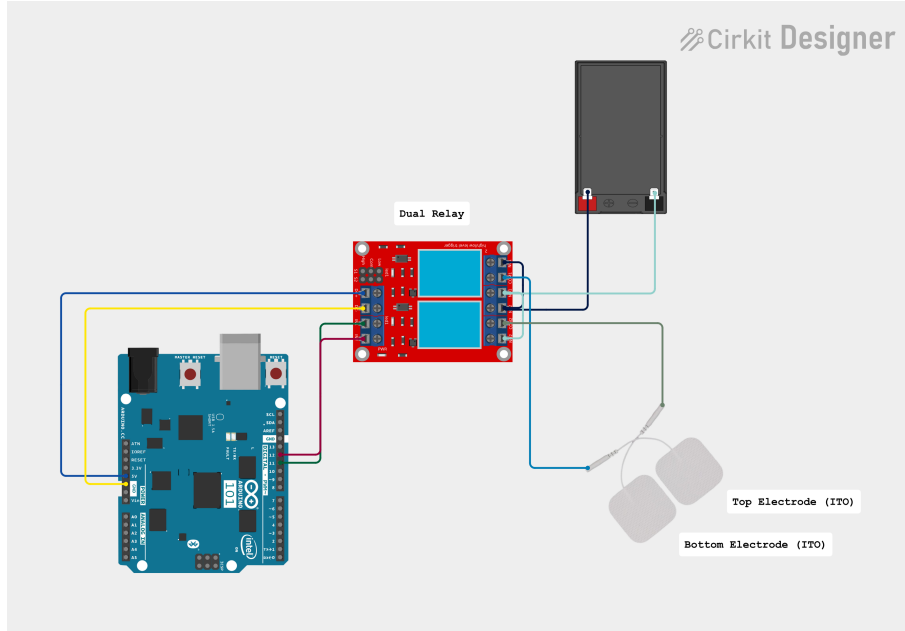
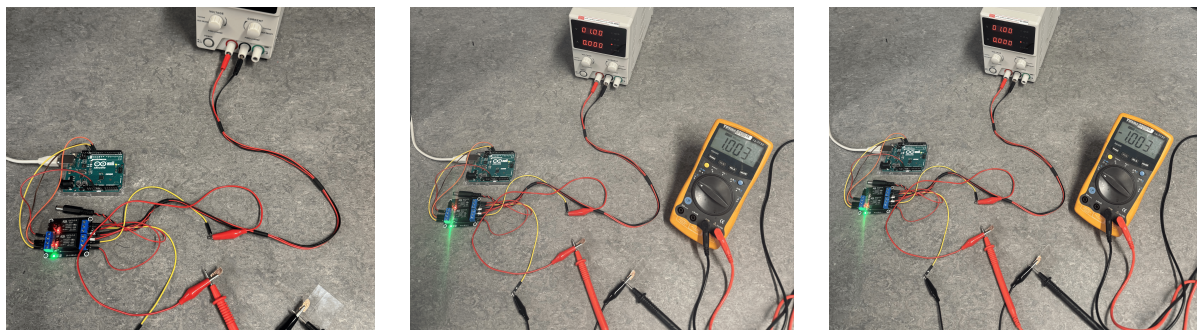


Figure 5.9: Electronic architecture of the single-segment display prototype.

Results And Discussion

To minimise the risk of damaging the display segment during testing, the applied voltage was limited to ± 1 V. Multimeter measurements were taken across the two electrodes while sending alternating black and white state commands. A positive voltage difference of approximately +1 V was recorded during the white state command, and a negative voltage difference of approximately -1 V was measured during the black state command. See Figure 5.10b and Figure 5.10c for representative measurements corresponding to the white and black states, respectively. These results confirm correct electrophoretic responsiveness for binary black-white switching of the device.



(a) Final assembled electronic architecture.

(b) Positive voltage difference (+1 V) during white state.

(c) Negative voltage difference (-1 V) during black state.

Figure 5.10: Verification of voltage polarity switching.

5.4.4 Integrated Hydrogel-Electrophoretic Display Stack

Materials

See Section 5.4.1 for the PAA/GE/E-Ink composite hydrogels fabricated based on optimised protocols. Samples prepared using the Photo-3 UV curing protocol (90 s exposure at 405 nm) were selected as the primary candidates for switching tests. Additional samples using Photo-1 (30 s), and Photo-2 (60 s) UV curing protocols were also tested for comparative evaluation. See Section 5.4.3 for the single-segment display prototype electronics used.

Method

Each hydrogel sample was placed between two ITO film electrodes within the prototype stack. The Arduino microcontroller was programmed to send alternating black-white switching commands to the relay module, in order to enable bidirectional voltage application across the hydrogel.

Initial electrophoretic switching tests were conducted using three small hydrogel-E-Ink test samples (Photo 1–3), placed on a single ITO film. These were tested sequentially under increasing voltages, starting at ± 1 V and incrementally raised to a maximum of ± 30 V (the upper safe limit for on-skin applications). Each sample was visually monitored before, during, and after voltage application to detect any signs of pigment migration or image formation. Based on the most promising formulation Photo-3 (Mix-4), a final prototype was subsequently fabricated in larger mold using the Photo-3 protocol. See Figure 5.11 for images of the electrophoretic test sequence and final prototype.

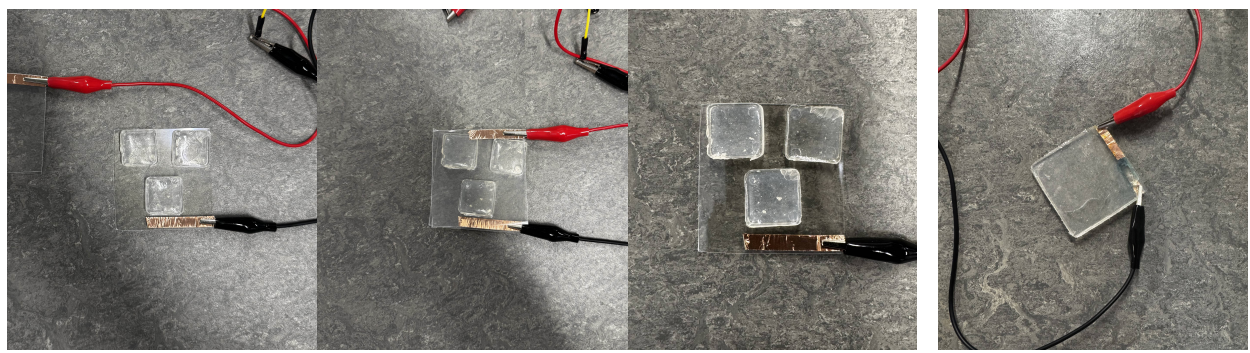


Figure 5.11: Electrophoretic switching test sequence. Panels (a)–(c) show three small hydrogel-E-Ink test samples (Photos 1–3) placed left to right on a single ITO substrate, captured before, during, and after application of up to ± 30 V. Panel (d) shows the final prototype fabricated using the same formulation and mixing conditions as Photo 3 (Mix-4 protocol), but cast in a larger mold. No visible colour switching was observed in any tests.

5.5 Results and Discussion

Unfortunately, no observable colour switching was detected in any of the tested samples, or the final prototype across the applied voltage range. This indicated that although the electronic control system successfully generated alternating electric fields, the embedded E-Ink microcapsules were not exhibiting electrophoretic movement.

Several potential explanations for the observed lack of switching were considered:

- Leakage of the electrophoretic active materials from the microcapsules over time, as the only available samples were over a year old, and this is a known issue with the current generation of biocompatible microcapsules used according to Wenda Zhao.
- Excessive mechanical rupture of microcapsules caused by mixing shear forces or UV photopolymerisation exposure, leading to loss of function. See Section 5.4.1 for details on microcapsule stability.

5.5. RESULTS AND DISCUSSION

- Incompatibility of the hydrogel matrix environment with electrophoretic operation, potentially impeding microcapsule response to the electric field.

Based on the microscopy observations and known vulnerabilities of the current generation of available biocompatible microcapsules used in testing, it is hypothesised that a combination of active material leakage, mechanical damage, and UV damage were the primary causes of switching failure.

There is significant scope for future work involving access to newer batches of current generation biocompatible microcapsules, and next-generation biocompatible microcapsules, either with enhanced mechanical strength to decrease mechanical degradation and active material leakage, or with increased resistance to photopolymerisation-induced degradation. Alternatively, evaluation of conventional, non-biocompatible E-Ink microcapsules, unavailable for the present study due to cost and time constraints, could be undertaken to determine whether the observed failures are primarily attributable to intrinsic microcapsule fragility or incompatibility with the hydrogel matrix.

If newer batches of biocompatible microcapsules, and conventional microcapsules also exhibit rupture under UV exposure, and if next-generation biocompatible, photopolymerisation-resistant microcapsules cannot be developed, alternative hydrogel systems should be explored. In particular, hydrogel formulations that avoid UV-based curing mechanisms could be synthesised to assess whether hydrogels, as a broader material class, are viable matrices for encapsulating and operating E-Ink microcapsules without compromising electrophoretic functionality.

Chapter 6

Conclusion

6.1 Summary

This work addresses the gap between recent advances in biocompatible electrophoretic materials, advances in flexible conductive materials, and the creation of a wearable E-Ink display. Through biocompatibility testing, we show that the biocompatibility of E-Ink microcapsules and associated materials can be evaluated through structured testing protocols, that conductive hydrogels can be designed to meet the mechanical, optical, and implicit biocompatibility requirements of wearable displays, and that material limitations in the current generation of biocompatible E-Ink microcapsules currently prevent the realisation of a wearable E-Ink display. In doing so our work lays the necessary groundwork for future research and development of a wearable E-Ink display, moving beyond traditional rigid applications, and ultimately towards, "digital tattoos."

We consolidate foundational knowledge across biocompatibility testing, electrophoretic display physics, and hydrogel design, creating a practical primer for researchers and developers pursuing wearable E-Ink displays. Up until now, this knowledge has been fragmented across diverse fields and scattered literature, making it difficult to access in a structured, application-focused form. We developed a conductive hydrogel specifically designed for wearable display applications, combining mechanical robustness, high transparency, high conductivity, and implied biocompatibility, that can be used for wearable displays.

We also fabricated and evaluated a stepping stone early prototype by embedding the current generation of biocompatible E-Ink microcapsules within our conductive hydrogel to open the way for future researchers and developers to create a wearable E-Ink display. Although a fully functional wearable E-Ink display was not achieved, our findings highlight critical challenges for future work, particularly mechanical fragility, UV instability, and potential leakage in the current generation of biocompatible E-Ink microcapsules.

In retrospect, an early-stage evaluation of the current generation of biocompatible microcapsules' UV stability could have prevented reliance on photopolymerisation as the hydrogel crosslinking method, which later proved incompatible. Long delays in sourcing chemicals, also restricted our ability to iterate rapidly or later explore a wider range of hydrogel formulations. As a result, we focused on developing one type of hydrogel that could be produced with minimal resources and under basic lab conditions, optimised for speed and simplicity.

6.2 Future Explorations

In science, outcomes that don't go as planned are not failures. They are essential steps in the process of discovery. When an experiment doesn't work, it often reveals unexpected behavior, hidden variables, or incorrect assumptions, all of which deepen our understanding. These moments prompt new questions, refine our methods, and guide future work more effectively than success alone sometimes can. We particularly propose the following structured roadmap as the next phase of the BioPixel research programme, outlining concrete, sequential projects that build on BioPixel's current display stack but address the challenges identified in our work, and can be pursued as a series of targeted research projects addressing

6.2. FUTURE EXPLORATIONS

specific parts, or as broader, multi-year PhD research programmes addressing major components of the platform and underlying materials.

- Investigate whether newer batches of biocompatible E-Ink microcapsules, and conventional E-Ink microcapsules (e.g., from FabricatInk upcycling [11]) exhibit the same material limitations as the biocompatible microcapsules used in our work by integrating them into our existing display stack, and testing performance.
- Explore new microcapsule formulations that are more mechanically robust, leak-resistant, and UV-stable to support long-term use in wearable E-Ink displays and "digital tattoos".
- Integrate the new generation of biocompatible E-Ink microcapsules into the display stack and evaluate performance.
- Develop a battery-powered wearable E-Ink display by subdividing the conductive hydrogel into individually addressable pixel regions to create a portable multi-matrix wearable E-Ink display.
- Test the biocompatibility of the complete display stack using standard assays (e.g., cytotoxicity, and sensitisation), and, if compatible, attempt to use human skin as the bottom electrode, to create a prototype "digital tattoo".
- Integrate thin-film transistor (TFT) arrays, and optimal driving waveforms for active matrix addressing to create a high resolution "digital tattoo".

Fundamentally, our work was a research focused material science project that attempted to build one novel technology, a wearable E-Ink display, on top of another novel and unproven technology, biocompatible E-Ink microcapsules. The layered risk ultimately reflects a broader shift in Human–Computer Interaction research, as we move beyond external wearables toward technologies that are more materially and functionally integrated with the body itself, where developing new forms of interaction increasingly requires deep engagement with the bleeding edge of materials science. Despite these constraints, we hope this work offers a foundational platform, practical insights, and inspiration for advancing the creation of a wearable E-Ink display and, ultimately, "digital tattoos".

Bibliography

- [1] Iso 10993-1:2018 – biological evaluation of medical devices – part 1: Evaluation and testing within a risk management process. <https://www.iso.org/standard/68936.html>, 2018. Corrected version 2018-10.
- [2] Iso 10993-10:2021 - biological evaluation of medical devices - part 10: Tests for irritation and skin sensitization. <https://www.iso.org/standard/75279.html>, 2021. Technical revision incorporating in vitro and in chemico methods in Annex C.
- [3] Iso/ts 11796:2023 - biological evaluation of medical devices - guidance on the conduct of in vitro skin sensitization validation studies for medical devices. <https://www.iso.org/standard/83916.html>, 2023.
- [4] Shouhong Chen, Bin Sun, Xiaorong Chen, et al. Electrophoretic display fluid, May 2016. United States Patent. URL: <https://patents.google.com/patent/US9341915B2/en>.
- [5] Chien-Hung Cheng, Chien-Chung Lin, Chih-Hsiung Wu, and Chih-Hsiang Lin. Thin film transistor array substrate and electronic ink display device, February 2012. URL: <https://patents.google.com/patent/US8115202B2/en>.
- [6] Decochrom. Decochrom. 2022. decochrom website, April 2023. URL: <https://decochrom.com>.
- [7] Christine Dierk, Molly Jane Pearce Nicholas, and Eric Paulos. Alterwear: Battery-free wearable displays for opportunistic interactions. In *Proceedings of the 2018 CHI Conference on Human Factors in Computing Systems*, CHI '18, page 1–11, New York, NY, USA, 2018. Association for Computing Machinery. [doi:10.1145/3173574.3173794](https://doi.org/10.1145/3173574.3173794).
- [8] Jagan Mohan Doddha, Kalim Deshmukh, Deon Bezuidenhout, and Y. Yeh. Hydrogels: Definition, history, classifications, formation, constitutive characteristics, and applications. In Jagan Mohan Doddha, Kalim Deshmukh, and Deon Bezuidenhout, editors, *Multicomponent Hydrogels: Smart Materials for Biomedical Applications*, Biomaterials Science Series, chapter 1, pages 1–35. Royal Society of Chemistry, 2023. URL: <https://books.rsc.org/books/edited-volume/2091/chapter/7582153/Hydrogels-Definition-History-Classifications>, doi:10.1039/9781837670055-00001.
- [9] Wei Gao, Deji Akinwande, and Nanshu Lu. Low-cost, m-thick, tape-free electronic tattoo sensors with minimized motion artifacts for continuous electrophysiology. *npj Flexible Electronics*, 2(1):1–12, 2018. URL: <https://www.nature.com/articles/s41528-017-0019-4>, doi:10.1038/s41528-017-0019-4.
- [10] Ollie Hanton, Mike Fraser, and Anne Roudaut. Displayfab: The state of the art and a roadmap in the personal fabrication of free-form displays using active materials and additive manufacturing. In *Proceedings of the 2024 CHI Conference on Human Factors in Computing Systems*, pages 1–24. ACM, 2024. [doi:10.1145/3613904.3642708](https://doi.org/10.1145/3613904.3642708).
- [11] Ollie Hanton, Zichao Shen, Mike Fraser, and Anne Roudaut. Fabricatink: Personal fabrication of bespoke displays using electronic ink from upcycled e readers. In *Proceedings of the 2022 CHI Conference on Human Factors in Computing Systems*, pages 1–15. ACM, 2022. [doi:10.1145/3491102.3501844](https://doi.org/10.1145/3491102.3501844).
- [12] Ollie Hanton, Michael Wessely, Stefanie Mueller, Mike Fraser, and Anne Roudaut. Protospray: Combining 3d printing and spraying to create interactive displays with arbitrary shapes. In *Proceedings of the 2020 CHI Conference on Human Factors in Computing Systems*, CHI '20, page 1–13, New York, NY, USA, 2020. Association for Computing Machinery. [doi:10.1145/3313831.3376543](https://doi.org/10.1145/3313831.3376543).

- [13] Tomoko Hashida, Yasuaki Kakehi, and Takeshi Naemura. Photochromic canvas drawing with patterned light. In *ACM SIGGRAPH 2010 Posters*, SIGGRAPH '10, New York, NY, USA, 2010. Association for Computing Machinery. [doi:10.1145/1836845.1836873](https://doi.org/10.1145/1836845.1836873).
- [14] Wenyao He, Zichuan Yi, Shitao Shen, Zhenyu Huang, Linwei Liu, Taiyuan Zhang, Wei Li, Li Wang, Lingling Shui, Chongfu Zhang, and Guofu Zhou. Driving waveform design of electrophoretic display based on optimized particle activation for a rapid response speed. *Micromachines*, 11(5):498, 2020. URL: <https://www.mdpi.com/2072-666X/11/5/498>, doi:10.3390/mi11050498.
- [15] Joseph M. Jacobson and Barrett Comiskey. Non emissive displays and piezoelectric power supplies therefor, July 27 1999. US Patent. URL: <https://patents.google.com/patent/US5930026A/en>.
- [16] Walther Jensen, Brock Craft, Markus Löchtefeld, and Pernille Bjørn. Learning through interactive artifacts: Personal fabrication using electrochromic displays to remember atari women programmers. *Entertainment Computing*, 40:100464, 2022. URL: <https://www.sciencedirect.com/science/article/pii/S1875952121000616>, doi:10.1016/j.entcom.2021.100464.
- [17] Yuhua Jin, Isabel Qamar, Michael Wessely, Aradhana Adhikari, Katarina Bulovic, Parinya Punpongpanon, and Stefanie Mueller. Photo-chameleon: Re-programmable multi-color textures using photochromic dyes. In *Proceedings of the 32nd Annual ACM Symposium on User Interface Software and Technology*, UIST '19, page 701–712, New York, NY, USA, 2019. Association for Computing Machinery. [doi:10.1145/3332165.3347905](https://doi.org/10.1145/3332165.3347905).
- [18] Helena Kandárová and Peter Pôbiš. The “big three” in biocompatibility testing of medical devices: Implementation of alternatives to animal experimentation—are we there yet? *Frontiers in Toxicology*, 5:1337468, 2024. URL: <https://www.frontiersin.org/articles/10.3389/ftox.2023.1337468/full>, doi:10.3389/ftox.2023.1337468.
- [19] Jin-Ho Kim, Sang-Hoon Lee, and Jin-Ho Park. Flexible electrophoretic display device and method of manufacturing the same, June 2016. Available at: <https://patents.google.com/patent/US20160187759A1/en>.
- [20] Richard D. LeCain, Ara N. Knaian, Steven J. O’Neil, Gregg M. Duthaler, Guy M. Danner, Robert W. Zehner, Alberto Goenaga, Benjamin Max Davis, Randolph W. Chan, Jonathan D. Albert, et al. Components and methods for use in electro-optic displays, January 2006. US Patent. URL: <https://patents.google.com/patent/US6982178B2/en>.
- [21] Markus Löchtefeld, Anna Dagmar Bille Milthers, and Timothy Merritt. Staging constructionist learning about energy for children with electrochromic displays and low-cost materials. In *Proceedings of the 20th International Conference on Mobile and Ubiquitous Multimedia*, MUM '21, page 73–83, New York, NY, USA, 2022. Association for Computing Machinery. [doi:10.1145/3490632.3490654](https://doi.org/10.1145/3490632.3490654).
- [22] Markus Löchtefeld, Walther Jensen, and Çağlar Genç. Prototyping of transparent and flexible electrochromic displays. In *Proceedings of the 20th International Conference on Mobile and Ubiquitous Multimedia*, MUM '21, page 179–181, New York, NY, USA, 2022. Association for Computing Machinery. [doi:10.1145/3490632.3497750](https://doi.org/10.1145/3490632.3497750).
- [23] Simon Olberding, Michael Wessely, and Jürgen Steinle. Printscreens: fabricating highly customizable thin-film touch-displays. In *Proceedings of the 27th Annual ACM Symposium on User Interface Software and Technology*, UIST '14, page 281–290, New York, NY, USA, 2014. Association for Computing Machinery. [doi:10.1145/2642918.2647413](https://doi.org/10.1145/2642918.2647413).
- [24] Simon Olberding, Michael Wessely, and Jürgen Steinle. Printscreens: Fabricating highly customizable thin-film touch-displays. In *Proceedings of the 27th Annual ACM Symposium on User Interface Software and Technology (UIST '14)*, pages 281–290. ACM, 2014. doi:10.1145/2642918.2647413.
- [25] Organisation for Economic Co-operation and Development. Oecd test no. 442e: In vitro skin sensitisation - in vitro skin sensitisation assays addressing the key event on activation of dendritic cells on the adverse outcome pathway for skin sensitisation. OECD Guidelines for the Testing of Chemicals, Section 4, Health Effects, 2024. Paragraph 26, Prediction Model. URL: <https://www.oecd.org/env/testguidelines>.

- [26] Roshan Lalintha Peiris and Ryohei Nakatsu. Temptouch: A novel touch sensor using temperature controllers for surface based textile displays. In *Proceedings of the 2013 ACM International Conference on Interactive Tabletops and Surfaces*, ITS '13, page 105–114, New York, NY, USA, 2013. Association for Computing Machinery. [doi:10.1145/2512349.2512813](https://doi.org/10.1145/2512349.2512813).
- [27] Roshan Lalintha Peiris, Mili John Tharakan, Owen Noel Newton Fernando, and Adrian David Cheok. Ambikraf. *Multimedia tools and applications*, 66(1):81–94, 2013. [doi:10.1007/s11042-012-1142-9](https://doi.org/10.1007/s11042-012-1142-9).
- [28] A. Pizzoferrato, C. R. Arciola, D. Granchi, et al. Cell culture methods for testing biocompatibility. *Clinical Materials*, 15:173–190, 1994. [doi:10.1016/0267-6605\(94\)90081-7](https://doi.org/10.1016/0267-6605(94)90081-7).
- [29] Djurre Sijbren Postma et al. Microcapsule compositions stabilized with viscosity control agents, March 2018. World Intellectual Property Organization Patent Application. URL: <https://patents.google.com/patent/WO2018053356A1/en>.
- [30] Parinya Punpongsanon, Xin Wen, David S. Kim, and Stefanie Mueller. Colormod: Recoloring 3d printed objects using photochromic inks. In *Proceedings of the 2018 CHI Conference on Human Factors in Computing Systems*, CHI '18, page 1–12, New York, NY, USA, 2018. Association for Computing Machinery. [doi:10.1145/3173574.3173787](https://doi.org/10.1145/3173574.3173787).
- [31] Isabel P. S. Qamar, Sabina W Chen, Dimitri Tskhovrebadze, Paolo Boni, Faraz Faruqi, Michael Wessely, and Stefanie Mueller. Chromoprint: A multi-color 3d printer based on a reprogrammable photochromic resin. In *Extended Abstracts of the 2022 CHI Conference on Human Factors in Computing Systems*, CHI EA '22, New York, NY, USA, 2022. Association for Computing Machinery. [doi:10.1145/3491101.3519784](https://doi.org/10.1145/3491101.3519784).
- [32] Isabel P. S. Qamar, Rainer Groh, David Holman, and Anne Roudaut. Hci meets material science: A literature review of morphing materials for the design of shape-changing interfaces. In *Proceedings of the 2018 CHI Conference on Human Factors in Computing Systems*, CHI '18, page 1–23, New York, NY, USA, 2018. Association for Computing Machinery. [doi:10.1145/3173574.3173948](https://doi.org/10.1145/3173574.3173948).
- [33] David Sweeney, Nicholas Chen, Steve Hodges, and Tobias Grosse-Puppeldahl. Displays as a material: A route to making displays more pervasive. *IEEE Pervasive Computing*, 15(3):77–82, 2016. [doi:10.1109/MPRV.2016.56](https://doi.org/10.1109/MPRV.2016.56).
- [34] Yakindra Prasad Timilsena, Taiwo O. Akanbi, Nauman Khalid, Benu Adhikari, and Colin J. Barrow. Complex coacervation: Principles, mechanisms and applications in microencapsulation. *International Journal of Biological Macromolecules*, 121:1276–1286, 2019. URL: <https://www.sciencedirect.com/science/article/pii/S0141813018348967>, [doi:10.1016/j.ijbiomac.2018.10.144](https://doi.org/10.1016/j.ijbiomac.2018.10.144).
- [35] Xuechuan Wang, Zhongxue Bai, Manhui Zheng, Ouyang Yue, Mengdi Hou, Boqiang Cui, Rongrong Su, Chao Wei, and Xinhua Liu. Engineered gelatin-based conductive hydrogels for flexible wearable electronic devices: Fundamentals and recent advances. *Journal of Science: Advanced Materials and Devices*, 7:100451, 2022. [doi:10.1016/j.jsamd.2022.100451](https://doi.org/10.1016/j.jsamd.2022.100451).
- [36] Michael Wessely, Yuhua Jin, Cattalyya Nuengsigkapian, Aleksei Kashapov, Isabel P. S. Qamar, Dzmitry Tsetserukou, and Stefanie Mueller. Chromoupdate: Fast design iteration of photochromic color textures using grayscale previews and local color updates. In *Proceedings of the 2021 CHI Conference on Human Factors in Computing Systems*, CHI '21, New York, NY, USA, 2021. Association for Computing Machinery. [doi:10.1145/3411764.3445391](https://doi.org/10.1145/3411764.3445391).
- [37] Michael Wessely, Ticha Sethapakdi, Carlos Castillo, Jackson C. Snowden, Ollie Hanton, Isabel P. S. Qamar, Mike Fraser, Anne Roudaut, and Stefanie Mueller. Sprayable user interfaces: Prototyping large-scale interactive surfaces with sensors and displays. In *Proceedings of the 2020 CHI Conference on Human Factors in Computing Systems*, CHI '20, page 1–12, New York, NY, USA, 2020. Association for Computing Machinery. [doi:10.1145/3313831.3376249](https://doi.org/10.1145/3313831.3376249).
- [38] Michael Wessely, Theophanis Tsandilas, and Wendy E. Mackay. Stretchis: Fabricating highly stretchable user interfaces. In *Proceedings of the 29th Annual Symposium on User Interface Software and Technology*, UIST '16, page 697–704, New York, NY, USA, 2016. Association for Computing Machinery. [doi:10.1145/2984511.2984521](https://doi.org/10.1145/2984511.2984521).

BIBLIOGRAPHY

- [39] Qi Xu, Zijian Wu, Wei Zhao, Mingpeng He, Ning Guo, Ling Weng, Zhiping Lin, Manal F Abou Taleb, Mohamed M Ibrahim, Man Vir Singh, et al. Strategies in the preparation of conductive polyvinyl alcohol hydrogels for applications in flexible strain sensors, flexible supercapacitors, and triboelectric nanogenerator sensors: an overview. *Advanced Composites and Hybrid Materials*, 6(1):203, 2023. [doi:10.1007/s42114-023-00783-5](https://doi.org/10.1007/s42114-023-00783-5).
- [40] Bo-Ru Yang and Kristiaan Neyts. *Fundamental Mechanisms of Electrophoretic Displays*, chapter 2, pages 31–50. John Wiley & Sons Ltd, 2022. URL: <https://onlinelibrary.wiley.com/doi/abs/10.1002/9781119745624.ch2>. [doi:10.1002/9781119745624.ch2](https://doi.org/10.1002/9781119745624.ch2).
- [41] Ying Yi, Mu Chiao, Khaled A Mahmoud, Lidong Wu, and Bo Wang. Preparation and characterization of pva/pvp conductive hydrogels formed by freeze-thaw processes as a promising material for sensor applications. *Journal of Materials Science*, 57(14):8029–8038, 2022. [doi:10.1007/s10853-022-07179-8](https://doi.org/10.1007/s10853-022-07179-8).
- [42] Hidekazu Yoshizawa. Trends in microencapsulation research. *KONA Powder and Particle Journal*, 22:23–31, 2004. URL: https://www.researchgate.net/publication/270559244_Trends_in_Microencapsulation_Research. [doi:10.14356/kona.2004009](https://doi.org/10.14356/kona.2004009).
- [43] Tianyu Yu, Weiyu Xu, Haiqing Xu, Guanhong Liu, Chang Liu, Guanyun Wang, and Haipeng Mi. Thermotion: Design and fabrication of thermofluidic composites for animation effects on object surfaces. In *Proceedings of the 2023 CHI Conference on Human Factors in Computing Systems*, CHI '23, New York, NY, USA, 2023. Association for Computing Machinery. [doi:10.1145/3544548.3580743](https://doi.org/10.1145/3544548.3580743).
- [44] Yixin Yuan, Jiulei Zhou, Guoqiang Lu, Jingxian Sun, and Liqun Tang. Highly stretchable, transparent, and self-adhesive ionic conductor for high-performance flexible sensors. *ACS Applied Polymer Materials*, 3(3):1610–1617, 2021. [doi:10.1021/acsapm.0c01442](https://doi.org/10.1021/acsapm.0c01442).

Appendix A

AI Prompts

1. I used ChatGPT to generate LaTeX code formatting chemical formulas and equation blocks. An example prompt was: “*What’s the correct LaTeX for COOH?*”
2. I used ChatGPT to generate LaTeX code for tables by providing it with the row and column headings I wanted, and a list of what I wanted in each row. An example prompt was: “*Create a LaTeX table with the following column and row headers with this data.*”
3. I used ChatGPT to generate LaTeX code for figures of images, including setting image size, width, and arrangements. I provided the image filenames, layout requirements, and figure dimensions. An example prompt was: “*Write LaTeX code so these three images are side by side in a row and all the same width and height*”
4. I used Perplexity to help identify relevant papers for my background sections. This included literature that cites ISO-10993, hydrogel classification, and the operational principles of E-Ink displays. Example prompts included: “*Source papers or textbooks detailing the classification and key characteristics of hydrogels,*” “*Find sources that explain how electrophoretic (E-Ink) displays work,*” and “*List papers that reference or apply ISO 10993 standards in biocompatibility testing.*”
5. I used Perplexity to assess whether the specific quantities of chemicals I planned to use in my hydrogel formulation, such as AA, GW, PEGDA, [BMIM]TfO, LAP, and D.M. Water were consistent with those typically reported in other papers. An example prompt was: “*Are the following concentrations for AA, GE, PEGDA, [BMIM]TfO, LAP, and D.M. Water typical in published papers on hydrogels? Give me sources.*”
6. I used Perplexity to clarify specific terms I read in papers. For example, when a paper referenced the “PAA backbone” I would prompt: “*What does ‘PAA backbone’ mean?*” Perplexity generated an explanation, and sources, which I read and used to better understand the paper I was reading, and write clearer descriptions in my dissertation.
7. I used Perplexity to source instructional videos demonstrating how to use relays, specifically the type I had selected for polarity switching. An example prompt was: “*Find a video of someone using this relay module to reverse polarity?*” The results primarily included videos showing how relays are used to reverse motor direction, which I watched to help build the polarity-switching setup in my own prototype.
8. I used Claude to generate a basic Arduino code snippet for polarity switching using a relay module. Claude generated the code which I then reviewed and edited based on how it performed in actual tests of my prototype. An example prompt was: “*Generate Arduino code to switch polarity using a SPDT relay module?*”
9. I used Claude to help improve the comments in my Arduino code. An example prompt was: “*Add better comments to this code*”
10. I used Overleaf’s built-in spellcheck and grammar tools throughout the document.

Appendix B

Code

The Arduino code used to control the BioPixel prototype is publicly available at: <https://github.com/bloomgithub/bio-pixel>.